Title

Oncogene Amplification in Growth Factor Signaling Pathways Renders Cancers Dependent on Membrane Lipid Remodeling

Journal

Cell Metabolism, 30(3)

ISSN

1550-4131

Authors

Bi, Junfeng
Ichu, Taka-Aki
Zanca, Ciro
et al.

Publication Date

2019-09-01

DOI

10.1016/j.cmet.2019.06.014

Peer reviewed

HHS Public Access

Author manuscript

Cell Metab. Author manuscript; available in PMC 2020 September 03.

Published in final edited form as:

Cell Metab. 2019 September 03; 30(3): 525–538.e8. doi:10.1016/j.cmet.2019.06.014.

Oncogene amplification in growth factor signaling pathways renders cancers dependent on membrane lipid remodeling

Junfeng Bi[1], **Taka-Aki Ichu**[2], **Ciro Zanca**[1], **Huijun Yang**[1], **Wei Zhang**[3], **Yuchao Gu**[1,4], **Sudhir Chowdhry**[1], **Alex Reed**[2], **Shiro Ikegami**[5], **Kristen M. Turner**[1], **Wenjing Zhang**[1], **Genaro R. Villa**[1,4], **Sihan Wu**[1], **Oswald Quehenberger**[3,6], **William H. Yong**[7], **Harley I. Kornblum**[4,8], **Jeremy N. Rich**[9], **Timothy F. Cloughesy**[7], **Webster K. Cavenee**[1,3,11], **Frank B. Furnari**[1,10,11], **Benjamin F. Cravatt**[2], **Paul S. Mischel**[1,10,11,12,*]

[1]Ludwig Institute for Cancer Research, University of California San Diego, La Jolla, CA 92093, USA

[2]Department of Chemistry, The Skaggs Institute for Chemical Biology, The Scripps Research Institute, La Jolla, CA 92037, USA

[3]Department of Medicine, UCSD School of Medicine, La Jolla, CA 92093, USA

[4]Department of Molecular and Medical Pharmacology David Geffen UCLA School of Medicine, Los Angeles, CA 90095, USA

[5]Department of Neurological Surgery, Chiba University Graduate School of Medicine, Chiba 260-8670, Japan

[6]Department of Pharmacology, UCSD School of Medicine, La Jolla, CA 92093, USA

[7]Department of Neurology, David Geffen School of Medicine, University of California Los Angeles, California 90095, USA

[8]Jonsson Comprehensive Cancer Center, David Geffen UCLA School of Medicine, Los Angeles, California, USA

[9]Division of Regenerative Medicine, Department of Medicine, University of California, San Diego, San Diego, CA, USA

[10]Department of Pathology, UCSD School of Medicine, La Jolla, CA 92093, USA

[11]Moores Cancer Center, UCSD School of Medicine, La Jolla, CA 92093 USA

[*]Correspondence: P.S.M. (pmischel@ucsd.edu).

Author Contributions

J.B., T. I., C. Z., H.Y., Y.G., S.C., A.R., K.M.T., W.Z., G.R.V., S.W., O.Q., B.F.C., and P.S.M. designed and performed experiments. H.I.K., W.H.Y., T.F.C., and F.B.F. provided samples or regents and intellectual input. J.N.R. and W.K.C. provided intellectual input. J.B., T.I., W. Z., S. I., O.Q., B.F.C., and P.S.M. analyzed and interpreted data. J.B. and P.S.M. wrote the manuscript.

Declaration of Interests

PSM is co-founder of Pretzel Therapeutics, Inc. He has equity and serves as a consultant for the company. PSM also did a one-time consultation for Abide Therapeutics, Inc.

[12]Lead Contact

Summary

Advances in DNA sequencing technologies have reshaped our understanding of the molecular basis of cancer, providing a precise genomic view of tumors. Complementary biochemical and biophysical perspectives of cancer point towards profound shifts in nutrient uptake and utilization that propel tumor growth and major changes in the structure of the plasma membrane of tumor cells. The molecular mechanisms that bridge these fundamental aspects of tumor biology remain poorly understood. Here, we show that the lysophosphatidylcholine acyltransferase LPCAT1 functionally links specific genetic alterations in cancer with aberrant metabolism and plasma membrane remodeling to drive tumor growth. Growth factor receptor-driven cancers are found to depend on LPCAT1 to shape plasma membrane composition through enhanced saturated phosphatidylcholine content that is, in turn, required for the transduction of oncogenic signals. These results point to a genotype-informed strategy that prioritizes lipid remodeling pathways as therapeutic targets for diverse cancers.

Graphical Abstract

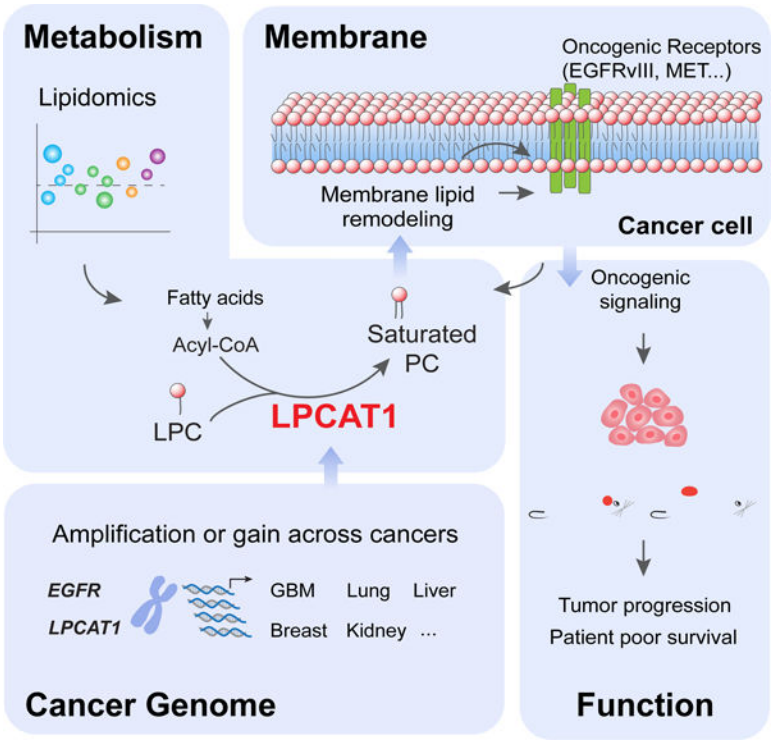

eTOC Blurb

Persistent growth factor receptor signaling and metabolic reprograming are hallmarks of cancer. Bi et al. show that LPCAT1-mediated phospholipid remodeling supports the sustained oncogenic activity of growth factor receptors on plasma membrane of tumor cells, suggesting an actionable dependency in a wide variety of cancers.

Introduction

Persistent survival signaling is a hallmark of cancer (Hanahan and Weinberg, 2011). Amplification of, and/or gain of function mutations in genes that encode key components of the growth factor signaling system, are among the most frequent genetic alterations in a diverse set of cancers (Sanchez-Vega et al., 2018), providing a compelling source of targetable driver oncogenes for cancer drug development. Amplified and mutated growth factor receptors, and associated mutated signaling proteins, reside primarily within or at the plasma membrane and enable tumor cells to become independent of external growth control cues. The plasma membrane of cancer cells is suspected to have major changes in its structure and organization to support growth factor signaling (Abercrombie and Ambrose, 1962). However, the biophysical and enzymatic mechanisms that determine how altered growth factor receptor signaling is regulated by, and regulates changes in plasma membrane composition in cancer, is not well understood.

The signaling activity of the plasma membrane is influenced by its biophysical properties, including curvature, charge, fluidity and local architecture. The clustering of signaling molecules into substructures, often referred to as lipid rafts, provides one such example (Lingwood and Simons, 2010; Sezgin et al., 2017). These biophysical properties depend on the specific constituents of the lipid bilayer, including phospholipids, sphingolipids and cholesterol (Harayama and Riezman, 2018; van Meer et al., 2008). Despite general agreement that the composition of phospholipids in the membrane can impact intracellular signaling by controlling membrane architecture, the molecular mechanisms that establish plasma membrane composition and structure in cancer are not well understood.

Not only can changes in the physical properties of the membrane change how growth factor receptors function, but growth factor signaling can also change the properties of the plasma membrane, creating feedforward mechanisms that drive sustained proliferative signaling. Growth factor receptor signaling, by altering nutrient uptake and metabolic pathway flux, can determine the specific lipid composition of cellular membranes, thus regulating their shape and fluidity and the corresponding clustering and activation of signaling complexes contained therein. Recent work, including from our group, demonstrates that altered growth factor receptor signaling in cancer can determine the levels of major lipid classes and the precursors from which they are formed (Guo et al., 2009; Guo et al., 2011; Pavlova and Thompson, 2016; Villa et al., 2016). Yet, the specific enzymes responsible for mediating these lipid changes and how they impart enhanced tumorigenicity remain poorly understood.

Here, we identify a critical, enzymatic link between some of the most common genomic alterations in the growth factor signaling system in cancer and reorganization of the plasma membrane. We show that lipid metabolic enzyme LPCAT1 is required for sustained proliferative signaling and demonstrate its association with poor outcome in patients. We further show that LPCAT1 controls membrane phospholipid saturation and is required for tumor growth *in vivo*, suggesting a potential new precision oncology approach to target a wide variety of growth factor-dependent cancers.

Results

EGFRvIII Signaling Alters the Phospholipid Composition of Tumor Cells through LPCAT1

We initially focused on EGFR because it is one of the most commonly amplified and/or mutated driver oncogenes in a wide variety of cancer types (Sanchez-Vega et al., 2018), and because molecular dynamic studies indicate that composition of plasma membrane phospholipids may be important in regulating EGFR activity (Arkhipov et al., 2013). We examined the impact of the constitutively active EGFR mutant, EGFRvIII, which is a common oncogenic driver in glioblastoma (GBM), on phospholipid composition by mass spectrometry-based lipidomics (Figures S1A and S1B). Transduction of EGFRvIII into U87 GBM cells significantly reduced lysophosphatidylcholine (LPC) species and increased saturated phosphatidylcholine (PC) levels (Figures 1A,1B and S1C), while concomitantly lowering the amount of intracellular free fatty acids (FFAs) (Figure S1D). This rise in saturated PC, concomitant with reductions in LPC and FFAs, raised the possibility that EGFRvIII might change phospholipid composition through the Lands cycle, a series of enzymatic reactions involving de-acylation of phospholipids followed by reacylation with different acyl-CoAs derived from FFAs. The Lands cycle is an efficient way for cells to generate a diversity of membrane phospholipids that may vary in a number of biochemical features, including saturation, from existing fatty acid pools (Hishikawa et al., 2014; Lands, 1958).

The reacylation phase of the Lands cycle in PC remodeling is catalyzed by a family of lysophosphatidylcholine acetyltransferases, LPCATs (LPCAT1-LPCAT4) (Harayama et al., 2014; Hishikawa et al., 2008). We detected a greater than two-fold rise in PC32:0 (PC16:0/16:0, 1, 2-dipalmitoyl-sn-glycero-3-phosphocholine, DPPC), a known major product of LPCAT1 (Harayama et al., 2014), in EGFRvIII-expressing cells (Figures 1A and S1E). Upregulation of LPCAT1 has been reported in multiple cancers and links phospholipid changes to cancer cell proliferation and invasiveness(Abdelzaher and Mostafa, 2015; Du et al., 2017; Mansilla et al., 2009; Morita et al., 2013; Shida-Sakazume et al., 2015; Uehara et al., 2016). In GBM, *LPCAT1* mRNA was significantly elevated relative to the other three LPCATs in an analysis of 273 GBM samples from the TCGA dataset (Figure S1F). Therefore, we examined the impact of LPCAT1 on phospholipid profiles by genetic depletion using shRNA (Figures S1G and S1H). LPCAT1 depletion significantly reduced saturated PCs including PC28:0, PC30:0 and PC32:0 and profoundly altered the saturated PC components of the lipid-lipid network (Figures 1C–1F and Table S1). The reduction in the fraction of saturated PCs correlated with an increase in the monounsaturated and polyunsaturated PCs fractions, and with a rise in both LPCs and FFAs (Figures 1G, S1I, and S1J). Taken together, these results demonstrate that EGFRvIII promotes PC saturation through LPCAT1.

LPCAT1 Is Highly Upregulated in EGFR-activated GBM Samples and Required for EGFR Signaling

Consistent with EGFRvIII-induced lipid changes, LPCAT1 protein and mRNA level are highly upregulated by EGFR signaling in GBM cells (Figures 2A–E and S2A). Immunohistochemistry analysis of a tissue microarray containing 93 GBM samples and

adjacent normal brain tissue cores, revealing that LPCAT1 protein level was significantly elevated in GBM tumor samples ($p < 0.01$) (Figures 2F and 2G), and its expression was highly correlated with phospho-EGFR ($p< 0.005$) and downstream signaling through known EGFR-dependent pathways ($p < 0.02$) (Figures 2H and S2B). Further, genetic depletion of LPCAT1 with shRNA knockdown in three GBM cell lines, including two patient-derived models that have endogenous EGFRvIII amplification (Nathanson et al., 2014; Turner et al., 2017), suppressed EGFR phosphorylation and downstream signaling (Figure 2I), which was rescued by addition of DPPC (PC16:0/16:0) liposomes and saturated C16:0 and C14:0 fatty acids (Figures 2J, 2K, S2C and S2D). Taken together, these results indicate that LPCAT1 is required for EGFR signaling through its effect on generating saturated PCs.

We next examined the impact of LPCAT1 on membrane structure. Saturated lipids are thought to contribute to the formation of ordered domains within the plasma membrane that contain active signaling complexes (Harayama and Riezman, 2018). However, the enzymatic mechanisms that link oncogenic growth factor receptor activity with changes in plasma membrane order and signal transduction are not well understood. We determined the effect of EGFRvIII and LPCAT1- plasma membrane order by staining giant plasma membrane vesicles (GPMVs) and live GBM cells with the lipid phase sensitive fluorescent probe Laurdan (Figures 2L–2N, S2E and S2F), which has been used to study membrane dynamics (Owen et al., 2011; Parasassi et al., 1997; Sezgin et al., 2012). Laurdan staining provides a quantitative read-out of the relative order of the plasma membrane based on shifts in the emission spectra profiles generated by probe binding to ordered vs. disordered phases of the plasma membrane (Owen et al., 2011; Parasassi et al., 1997; Wang et al., 2016). EGFRvIII significantly increased the plasma membrane order, which was fully abrogated by shRNA-mediated genetic depletion of LPCAT1 (Figures 2L–2N, S2E and S2F). DPPC liposomes addition could fully rescue the membrane order of GBM cells after LPCAT1-depletion (Figures 2M, 2N, S2E and S2F). These results demonstrate that EGFRvIII-dependent changes in phospholipid composition that are catalyzed by LPCAT1, regulate plasma membrane order.

Plasma membrane localization of EGFR has been shown critical for receptor activity and signal transduction (Tomas et al., 2014). Thus, we examined EGFR localization by imaging and flow cytometry in the patient-derived GBM cell isolates, in response to LPCAT1 shRNA treatment. Remarkably, LPCAT1 genetic depletion shifted EGFR from the plasma membrane to intracellular membrane compartments by stimulating receptor internalization (Figures 2O–2Q), which was rescued by feeding cells with DPPC liposomes (Figures 2O–2Q). LPCAT1 depletion did not induce phosphorylated p38 MAPK (Figure S2G), which indicates the increase of EGFR internalization after LPCAT1 depletion might be independent of p38 MAPK-mediated EGFR trafficking (Zwang and Yarden, 2006). EGFR has been shown to localize in lipid rafts that enriched with saturated phospholipids, including DPPC (PC16:0/16:0) (Pike et al., 2005). Thus, we performed the detergent-free fractionation of GBM cells, which shows a significant shift of EGFRvIII from lipid rafts fractions to non-rafts fractions (Figures S2H and S2I), suggesting a role of LPCAT1-mediated lipid saturation in maintaining lipid rafts association of EGFRvIII in cancer cells. These results provide a mechanistic link between the LPCAT1-dependent biochemical

changes in saturated PC composition, plasma membrane structure, and EGFR localization and signaling in cancer.

LPCAT1-saturated PC Axis Is Required for GBM Cell Survival and Growth

Next, we examined the impact of LPCAT1 genetic depletion on the relative cell viability and colony formation of GBM cells. LPCAT1 knockdown greatly decreased the viability of U87EGFRvIII cells and patient-derived GBM39 and HK301 cultures (Figures 3A and 3B). Under anchorage-independent conditions in soft agar, LPCAT1 knockdown abrogated colony formation, which was rescued by an shRNA-resistant LPCAT1 construct (Figures 3C and 3D). LPCAT1 depletion also significantly reduced the sphere diameter (Figures 3E and 3F). We also generated an inducible shRNA LPCAT1 knockdown system, which similarly reduced numbers of colonies formed in soft agar (Figures S3A–S3C).

To confirm that the LPCAT1-dependent reduction in GBM growth and colony formation was mediated by the loss of saturated PCs, we determined the ability of saturated (DPPC, PC16:0/16:0), monounsaturated (POPC, PC16:0/18:1, 1-palmitoyl-2-oleoyl-sn-glycero-3-phosphocholine), or polyunsaturated (PAPC, PC16:0/20:4, 1-palmitoyl-2-arachidonoyl-sn-glycero-3-phosphocholine) PCs to restore tumor cell viability after LPCAT1 knockdown. DPPC effectively rescued cell viability and colony formation in soft agar, whereas POPC, PAPC were not sufficient to rescue LPCAT1-deficient GBM cells (Figures 3G and 3H). As predicted by our hypothesis, LPC16:0 also could not rescue the viability of LPCAT1-deficient GBM cells (Figure 3G). In contrast, a constitutively active AKT allele bearing an E17K mutation, restored GBM colony formation and cell viability (Figures 3I–3K and S3D), consistent with the role for AKT in mediating EGFRvIII-dependent tumor growth (Cloughesy et al., 2014). Taken together, these results suggest that LPCAT1 promotes GBM growth by increasing saturated PC levels to maintain EGFR signaling.

LPCAT1 Depletion Suppresses Tumor Growth and Prolongs the Survival of Mice Bearing Intracranial Patient-Derived GBMs

To determine whether LPCAT1 is required to sustain the growth of EGFR-dependent GBMs *in vivo*, we introduced a doxycycline-inducible LPCAT1-shRNA construct, or a non-targeting control, into patient-derived GBM39 cells expressing the near-infrared fluorescent protein 720 (IRFP720), to facilitate non-invasive tumor monitoring in the brains of mice (Villa et al., 2016) (Figures 4A and S4A). Once tumors in the brain became detectable, mice were placed on a diet containing doxycycline and this caused a striking suppression of tumor growth upon LPCAT1 depletion ($p < 0.001$) (Figures 4B and 4C). Induced genetic depletion of LPCAT1 resulted in a highly significant, although not complete, reduction in LPCAT1 protein levels, which correlated with significant inhibition of EGFR phosphorylation, NDRG1 phosphorylation and Ki67 staining, and with a significant increase in tumor cell death ($p < 0.01$), as measured by a TUNEL assay (Figures 4D, 4E and S4B). Further, inducible genetic depletion of LPCAT1 significantly enhanced mouse survival ($p = 0.0013$) (Figure 4F). These results demonstrate that LPCAT1 is required for GBM growth in a clinically relevant patient-derived, orthotopic GBM model.

LPCAT1 Is Frequently Amplified and Associated with Shorter Patient Survival in a Wide Range of Cancers

Because aberrant growth factor receptor signaling is common in many types of cancer, not just GBM, we reasoned that LPCAT1 could potentially be important in a wide spectrum of cancer types. Genomic analysis of publicly available cancer sequencing databases of clinical samples and the cancer cell line encyclopedia (CCLE) revealed that *LPCAT1* copy number was increased in over 30% of pan-cancer patients and some of the most aggressive cancers, including lung adenocarcinoma and squamous carcinoma, ovarian cancers, bladder cancers, and invasive breast cancers (Figures 5A and 5B), in association with elevated LPCAT1 gene expression (Figures 5C, S5A and S5B). Elevated LPCAT1 gene expression, defined as a value greater than the top quartile level for the set, was associated with significantly worse disease-free survival in a pan-cancer analysis of 9502 patients ($p = 0.0072$) (Figure 5D). Increased *LPCAT1* expression also showed significant correlation with disease-free survival of lung cancer patients ($p = 0.0011$) (Figure 5E). This adverse association between elevated *LPCAT1* expression and overall survival was similarly detected across multiple tumor types, including renal cancer, hepatocellular carcinoma, cervical cancer and uveal melanoma (Figures 5F–5H and S5C). *LPCAT1* is frequently co-amplified with *TERT*, which is also located on chromosome 5 (5p15.33) (Figure S5D). However, no significant association between *LPCAT1* and *TERT* gene expression was found (Figure S5E), and unlike *LPCAT1*, *TERT* amplification did not confer shorter survival in patients with lung cancer, hepatocellular carcinoma and cervical cancer (Figures S5F–S5H). These results demonstrate that elevated *LPCAT1* DNA copy number and increased *LPCAT1* expression are associated with poor outcome in patients, independent of *TERT*. Unlike *LPCAT1*, three other genes of *LPCATs* family, *LPCAT2*, *LPCAT3* and *LPCAT4* (Cotte et al., 2018; Kurabe et al., 2013; Wang et al., 2018), were not commonly amplified in TCGA cancer datasets (Figure 5I). Notably, *LPCAT1*-amplified tumors showed a remarkably high level of co-amplification and mutations in genes encoding known oncogenic growth factor receptors and their key signaling intermediates (Figure 5H and Table S2), suggesting that LPCAT1 may be a potential target in some growth factor receptor-driven cancers.

LPCAT1 Depletion Effectively Kills a Wide Variety of *LPCAT1* Copy-number Increased Cancers via Its Effect on Saturated PC Synthesis

To assess the potential therapeutic relevance of the adverse survival association of increased *LPCAT1* copy number, we determined the impact of genetic depletion of LPCAT1 by shRNA knockdown in 18 tumor cell lines, and 2 non-cancer cell lines, profiled for *LPCAT1* DNA copy number (Figure S6A). Remarkably, genetic depletion of *LPCAT1* dramatically decreased the viability of *LPCAT1*-amplified tumor cell lines, and to a lesser extent tumor cells with *LPCAT1* copy gain, of various histological types (Figures 6A and S6B–S6D). Further, in the H1437 lung cancer cell line bearing *LPCAT1* gene amplification, DPPC (PC16:0/16:0) rescued colony formation, providing a mechanistic basis for our findings and confirming that LPCAT1 was required for tumor growth by generating saturated PCs (Figures 6B and 6C). Further consistent with our hypothesis that saturated PCs generated by LPCAT1 are required for growth factor receptor signaling in tumor cells, in H1437 lung cancer cells that also have a c-MET gain of function mutation (Ma et al., 2005; Ma et al.,

2003), shRNA-mediated *LPCAT1* knockdown abrogated MET phosphorylation and downstream signaling (Figure 6D).

To determine whether LPCAT1 is required for the growth of *LPCAT1*-amplified tumors *in vivo*, we introduced the doxycycline inducible *LPCAT1* shRNA into H1437 lung cancer cells (Figures S6E and S6F) and A498 renal cancer cells (Figure S6G). In subcutaneous xenografts, inducible genetic depletion of LPCAT1 abrogated tumor growth, blocked tumor cell proliferation as measured by Ki67 staining, and caused significant tumor cell death as detected by TUNEL staining (Figures 6E–6H and S6H). Importantly, an shRNA-resistant *LPCAT1* construct completely rescued the biochemical activity and *in vivo* growth of LPCAT1-depleted H1437 lung cancer cells (Figures S6E, S6F and 6F-6H). Inducible LPCAT1 shRNA similarly abrogated the growth of A498 renal cancer cells, although not quite as durably (Figures 6I and S6I). These results demonstrate that LPCAT1 is required for the *in vivo* growth of multiple *LPCAT1* copy-number gained or amplified cancers of different histological types.

Discussion

Here, we show that lysophosphatidylcholine acyltransferase LPCAT1 links altered cancer genomes with aberrant metabolism and plasma membrane remodeling to drive tumor growth through the production of saturated PCs (Figure 7). These results highlight LPCAT1 as a critical node integrating genetically altered growth factor receptor signaling with lipid remodeling to alter the physical properties of the plasma membrane and create a pro-tumor cellular state.

We initially sought to identify lipid modifying enzymes that could integrate persistent growth factor receptor signaling with plasma membrane remodeling by examining the impact of constitutive EGFR signaling on phospholipid composition in a simple cancer cell line model. This choice was motivated by the high frequency of EGFR amplification and mutation in cancer, and the potential importance of membrane phospholipids in regulating the activity of this receptor tyrosine kinase (Arkhipov et al., 2013; Pike et al., 2005). We not only demonstrated that LPCAT1 is a critical co-dependency target in EGFRvIII amplified GBMs, but also noted the high frequency of *LPCAT1* amplification or gain in many other cancer types, including those with mutations in the growth factor signaling system, which may explain its elevated mRNA and protein levels observed in clinical samples (Abdelzaher and Mostafa, 2015; Du et al., 2017; Morita et al., 2013).

The plasma membrane is not a uniform structure, but rather, is composed of distinct localized domains that differ in their lipid composition, structure, and signaling activity, and can be dynamically regulated by specific lipid-lipid and lipid protein interactions (Harayama and Riezman, 2018; Sezgin et al., 2017). Multiple biosynthetic pathways, and the lipids that they generate, may contribute to the unique membrane composition of cancer cells. Fatty acid synthesis, mobilization, and uptake are upregulated in many cancers (Currie et al., 2013; Nomura et al., 2010; Rohrig and Schulze, 2016), providing acyl groups that contribute to the wide array of membrane and signaling lipids that support tumorigenesis. De novo lipogenesis mediated membrane lipid saturation has been linked to the sensitivity of cancer

cells to free radicals and chemotherapeutics (Rysman et al., 2010). Cholesterol and sphingolipids, which alter the formation of lipid rafts, are also critical for tumor pathogenesis (Guo et al., 2011; Guri et al., 2017; Ogretmen, 2018; Villa et al., 2016). Phospholipids may also be important in determining the signaling properties of the plasma membrane of cancer cells, at least in part by regulating interactions between signaling proteins (Arkhipov et al., 2013; Wang et al., 2014; Zhou et al., 2017). Here we show that saturated PCs determine membrane order and are critical for permitting proliferative signaling that is activated by oncogenic growth factor receptor mutations, and we demonstrate that LPCAT1 is required for generating these saturated PCs in cancer. We further confirm that PC32:0, PC28:0 and PC30:0 are LPCAT1 products and demonstrate that LPCAT1-derived saturated PCs are required for tumor growth. Of note, these saturated PCs were previously shown to be associated with aggressive histology and poor outcome in a large cohort of breast cancer patients (Hilvo et al., 2011). This shift toward saturated phospholipids induced by LPCAT1 overexpression in cancer cells, may well reflect the substrate specificity of LPCAT1 (Nakanishi et al., 2006). Further, we show that the LPCAT1-mediated shift towards saturated phospholipids regulates EGFRvIII signaling, by controlling the amount of EGFRvIII on the plasma membrane, including by decreasing receptor internalization and increasing EGFRvIII association with lipid rafts. These results are consistent with previous studies suggesting that the state of phospholipid saturation in the plasma membrane may be important for maintaining lipid rafts and limiting receptor internalization (Pinot et al., 2014; Rajendran and Simons, 2005). Further, supporting the importance of saturated PCs in tumor pathogenesis, LPCAT3, which selectively incorporates polyunsaturated fatty acids into PCs and consequently reduces saturated PC levels in the membrane (Hashidate-Yoshida et al., 2015; Wang et al., 2016), suppresses intestinal tumorigenesis in mice carrying mutations in tumor suppressor gene *Apc* (Wang et al., 2018). These findings highlight the complex interplay of different LPCATs in determining the aggressive behavior of cancer cells by regulating PC saturation to control membrane structure and signaling activity.

New cancer drug development efforts aimed at identifying metabolic co-dependencies must consider not only the effect of target inhibition on tumor cells, but also its impact on normal cell physiology. *Lpcat1* knockout mice are viable in B6 background (Harayama et al., 2014), raising the possibility that a wide therapeutic window may exist for the development of LPCAT1 inhibitors. Possible adverse effects, such as respiratory failure and retinal degeneration that were reported in knockout mice of different genetic backgrounds (Bridges et al., 2010; Friedman et al., 2010), upon LPCAT1 inhibition should also be considered. Our additional findings that *LPCAT1* copy gain renders tumors, in particular growth factor-driven cancers, dependent on LPCAT1 for growth and survival, suggests a genotype-informed patient selection strategy, motivating the development of LPCAT1 inhibitors as candidate therapeutics for the wide spectrum of patients with *LPCAT1*-amplified, growth factor signaling-dependent cancers.

Limitations of Study

Our study demonstrates an important and potentially actionable role for LPCAT1 in cancer, linking oncogenic growth factor receptor signaling with dynamic membrane lipid

remodeling, to drive aggressive tumor growth. Future studies will be needed to further delineate the epigenetic, transcriptional, and possibly post-translational mechanisms by which oncogenic signaling controls LPCAT1 level. In addition, a deeper understanding of how specific phospholipids regulate the clustering and activation of amplified or mutated growth factor receptors in cancer, will be needed to better resolve the potentially targetable changes in the plasma membrane that are involved in cancer pathogenesis. Lastly, additional work will be required to identify, develop, and test new compounds for targeting LPCAT1 in cancer patients.

STAR Methods

Contact for Reagent and Resource Sharing

Further information and requests for resources and reagents should be directed to and will be fulfilled by the Lead Contact, Paul S. Mischel (pmischel@ucsd.edu)

Experimental Model and Subject Details

Cell Lines—All cell lines of this study are listed in the Key Resources Table. Human cancer cell lines U87, H1437, H1650, A549, Capan1, YAPC, Caki1, DU145, PC-9, PC-3, SN12C, H23, neurosphere lines GBM39 and HK301 were derived from male cancer patients, whereas human cancer cell lines H1734, HCC1954, T47D, CAOV3, OVCAR3, OVCAR8, SKMEL5, A498, non-cancer lines IMR90 and RPE1 were derived from female. GBM39 and HK301 patient-derived neurosphere lines were cultured in DMEM/F12 medium supplemented with 1x B27, 20 ng/ mL of EGF, 20 ng/ mL of FGF, 1 μg/ mL heparin and 1x Glutamax. GBM neurosphere lines were previously established as described (Nathanson et al., 2014). All patient tumor tissues to derive neurospheres were obtained under IRB approval with explicit informed consent from patients. The U87EGFRvIII isogenic cell line was established as previously described (Wang et al., 2006). Briefly, human EGFRvIII was transduced into U87 cells through a retroviral expression system. Cells stably expressing EGFRvIII were then selected by hygromycin and expanded for further experiments. The human glioma cell lines U87 and U87EGFRvIII were maintained in DMEM supplemented with 10% FBS and 1% penicillin/streptomycin. Normal Human Astrocytes (NHA) were cultured according to the manufacturer's standard protocol by using the AGM BulletKit. H1437 cells and other cell lines that are not mentioned above were all cultured in RPMI1640 supplemented with 10% FBS and 1% penicillin/streptomycin. For doxycycline-inducible experiments, cells were cultured in medium supplemented with 10% tet-free FBS and 1% penicillin/streptomycin. Attached cells were maintained in 10% FBS medium and changed to 1% FBS medium for further experiments as indicated in the methods. All cell lines were maintained in a humidified incubator with 5% CO_2 at 37°C.

Intracranial and Subcutaneous Xenograft Models—For the GBM orthotopic xenograft model, patient-derived neurosphere GBM39 cells were engineered to express near-infrared fluorescent protein IRFP720 and carrying vectors of inducible control or LPCAT1-targeting shRNAs. 2.5×10^5 of GBM39 cells in 5 μL PBS were intracranially injected into five-week-old female athymic nude mice (Charles River Laboratories) using a stereotactic system. Seven mice were injected for each group. Dox diet (Bio-Serv) was given

at day 4 after injection. Tumor growth was monitored once a week by using an FMT 2500 fluorescence tomography system (PerkinElmer). Survival until the onset of neurologic symptoms was applied for survival curves.

For subcutaneous xenograft models, H1437 and A498 cells were infected with lentivirus carrying inducible shRNA vectors and selected by puromycin treatment for 5 days in medium supplemented with 10% tet-free FBS. 10^6 of H1437 cells in 100 μL PBS, or 10^6 of A498 cells in 100 μL PBS with 50% matrigel (Corning), were subcutaneously injected into five-week-old female athymic nude mice (Charles River Laboratories). Dox diet (Bio-Serv) was given when tumors were established at day 4 after implantation. Eight tumors were injected for each group. For the genetic rescue group, a Flag-tagged wild-type form of LPCAT1 was stably expressed in H1437 cells carrying inducible LPCAT1#1 shRNA vectors. Mice weight and tumor size were measured every three days. Tumor volume was calculated by the formula: *½ x Length x Width x Height*. Mice were housed in a conventional barrier facility on a 12-hour light/dark cycle at 22°C with free access to water and food. Mice health status was checked by following the protocols. All mice experiments were performed according to the protocols approved by the Institutional Animal Use and Care Committee at University of California at San Diego.

Human GBM Tumor Tissue Microarray—Tissue microarrays were constructed as reported previously (Guo et al., 2009). Briefly, the representative tumor tissue cores and adjacent normal brain tissue cores were extracted with a 0.6-mm needle from the paraffin-embedded tissue blocks of primary GBM patients, and placed in a grid pattern into two recipient paraffin blocks, from which tissue sections were cut for further immunohistochemical analysis. All samples of the GBM tissue microarrays were obtained and approved under the UCLA IRB# 10–000655 (formerly known as UCLA IRB# 99–07-061). Immunohistochemical staining was performed to analyze the expression level of LPCAT1, pEGFR, pAKT, pS6, and pNDRG1 in 70 GBM tumor samples and 27 adjacent normal brain tissue samples. Images of stained tissue sections were reviewed and scored by a pathologist in a double-blind fashion.

Method Details

Lentivirus-mediated Gene Expression and RNA Interference—Lentivirus LPCAT1 expression plasmid pLVX-LPCAT1 was generated by cloning the full-length coding sequence of *LPCAT1* into a pLVX-Puro vector (XhoI and EcoRI). The shRNA-resistant version of *LPCAT1* was achieved by a series of point-mutations on the third nucleotide of amino acids in the shRNA#1-targeting sequence without changing amino acids (resistant sequence, CCAGACCAAACGCACTTTGAG), and then inserted into a pLVX-Puro vector (EcoRI and BamHI). Lentivirus constitutive active AKT1 expression plasmid pLVX-puro-HA-AKT-E17K-CA was generated by cloning the sequence of HA-AKT-E17K into a pLVX-Puro vector (XhoI and EcoRI). A FLAG-tag coding sequence was added in frame in front of the *LPCAT1* coding sequence and then cloned into a pLVX-Puro vector (EcoRI and BamHI) to get a pLVX-Flag-LPCAT1 plasmid. Lentivirus shRNA plasmids were purchased from Sigma and doxycycline-inducible shRNA plasmids were purchased from Dharmacon. For virus production, lentiviral plasmids were transfected into HEK293T

cells with lentivirus packaging plasmids (Clontech), and supernatant medium containing virus was collected at 72 hours after transfection. Virus titer was checked before use. Cells were infected with lentivirus overnight and medium was changed after infection. Infection efficiency and puromycin concentrations were determined for each cell line. In doxycycline-inducible shRNA experiments, cells were cultured in 10% tet-free FBS medium and selected by puromycin treatment for 5 days after infection. 0.5 μg/ mL of doxycycline was added and refreshed every three days to induce shRNA expression.

Gene Knockdown by siRNA—20 nM negative control siRNA or LPCAT1 ON-TARGETplus SMARTpool siRNA (Dharmacon) was transfected into U87 or U87EGFRvIII cells using the lipofectamine RNAiMAX transfection regent (ThermoFisher Scientific). Medium was replaced by fresh growth medium supplemented with 1% FBS after 24 hours of transfection, and cells were harvested after 5 days for western blot analysis.

Cell Viability and Cell Death Assays—Cells were seeded in 6-well plates (attached cells) or 0.25 cm^2 flasks (neurosphere cells) and cultured for six days. Live cells in each well or flask were counted by trypan blue assay using a TC10 automatic cell counter (Bio-Rad). Cell death was determined by using a FITC Annexin V Apoptosis Detection Kit (BD Biosciences). Briefly, cells were reseeded in 6 cm dishes at 48 hours after shRNA-virus infection and cultured in growth medium supplemented with 1% FBS for five days. Cells were then trypsinized down and combined with media supernatant. After spinning down, cells were resuspended and Annexin V/ PI staining was performed. Samples were then analyzed by flow cytometry using a BD LSRII flow cytometer (BD Biosciences).

Soft-agar Colony Formation Assay—2000 cells were mixed with 0.4% low-gelling-temperature agarose (Sigma) in growth medium and plated on a solidified bottom layer of 1% low-gelling-temperature agarose in growth medium in each well of 12-well plates. Three to four replicates were performed for each shRNA or treatment condition. Cells were fed with fresh growth medium every three days. Colonies were stained with 0.005% Cristal Violet solution after 4 weeks and imaged by a ChemiDoc imaging system (Bio-Rad). Colony numbers were counted by ImageJ.

Crystal Violet Clonogenic Assay—1000 or 2000 cells for each well were seeded into 6-well plates and cultured in 2 mL of growth medium for 2 weeks. Doxycycline (0.5 μg/mL) was added and refreshed every three days in inducible shRNA experiments. 10 μM of PC liposomes were added and medium was refreshed every four days. For crystal violet staining, medium was removed, and colonies were fixed with fixation solution (80% methanol in ddH_2O) for 10 min and stained with 0.05% crystal violet for 20 minutes. After washing with water and dried at room temperature overnight, plates were imaged by a ChemiDoc imaging system (Bio-Rad). Colony density was quantified by ImageJ.

RNA Extraction and qRT-PCR—Total RNA was extracted using the RNeasy Mini Kit and a total of 1 μg RNA for each sample was used for cDNA synthesis. RT-PCR was then performed using the SYBR Green Supermix (Bio-Rad, #1708880) on a CFX96 Real-Time PCR Detection System (Bio-Rad) by following the manufacturer's instructions. Results

were analyzed by the delta delta Ct method and normalized to the reference gene and indicated control group.

Western Blot Analysis—Cultured cells were washed with PBS and lysed with 1x RIPA lysis buffer supplemented with Halt Protease and Phosphatase Inhibitor Cocktail. Tumor samples were firstly homogenized on ice with cold PBS supplemented with Halt Protease and Phosphatase Inhibitor Cocktail and lysed by adding an equal amount of 2x RIPA buffer. Protein concentration of each sample was determined by using a BCA Protein Assay Kit (ThermoFisher Scientific). Equal amounts of protein extracts were mixed with sample buffer and boiled at 100°C for 5 minutes. Samples were separated by electrophoresis on 4%–12% NuPAGE Bis-Tris Mini Gel, and then transferred onto nitrocellulose membranes using the Trans-Blot Turbo Transfer System (Bio-Rad). Membranes were then blocked with 5% BSA in TBST buffer and incubated with corresponding primary antibodies (at 4°C overnight and HRP-conjug ated secondary antibodies at room temperature for 1 hour. The signal was developed with SuperSignal West Pico PLUS Chemiluminescent Substrate and captured using the ChemiDoc MP Imaging system (Bio-Rad).

Immunohistochemistry Analysis—Formalin-fixed, paraffin-embedded tumor tissue sections were prepared by the Histology Core Facility at UCSD Moores Cancer Center. Standard procedures of immunohistochemistry staining were followed. Antigen was retrieved by boiling slides in 0.01 M of pH 6.0 sodium citrate in a microwave for 15 minutes. Tissue sections were then incubated with corresponding primary antibodies at 4°C overnight, followed by 30 -minutes incubation with biotinylated secondary antibodies at room temperature. For TUNEL staining, tissue sections were incubated with TdT/ dUTP at 37°C for 30 minutes and then incu bated at room temperature with HRP-conjugated anti-Digoxigenin for 30 minutes after washing. Four representative images from each stained section were captured using an Olympus BX43 microscope. Staining intensity was then quantified by a pathologist in a double-blind fashion using Visiopharm image analysis software.

Density Gradient Fractionation—The method for detergent-free density gradient fractionation has been described previously (Cizmecioglu et al., 2016; Macdonald and Pike, 2005). In brief, cells grown in 1% FBS for three days were washed by cold PBS and scraped into the homogenization buffer (20 mM Tris-HCl, pH7.8, 0.250 M sucrose, 1 mM $CaCl_2$ and 1 mM $MgCl_2$). Cells were pelleted at 250 g for 5 minutes at 4°C and resuspended in 600 μl of cold homogenization buffer with protease and phosphatase inhibitors. Homogenates were then passed through a 23 g needle for 20 times and centrifuged at 1000 g for 10 min. The supernatants were collected in new 1.5 ml tubes and the pellets were again lysed by 400 μl cold homogenization buffer with protease and phosphatase inhibitors followed by passing 20 times through a 23 g needle. After centrifugation at 1000 g for 10 min at 4°C, two supernatants were combined for each sample and mixed with 1 ml of 50% Opti-Prep solution (Sigma). The mix was placed in the bottom of a 5 ml Ultra-Clear centrifuge tube (Beckman Coulter), and 400 μl each of 20%, 17.5%, 15%, 12.5%, 10%, 7.5% and 5% Opti-Prep solutions were poured on top. The tubes were then centrifuged for 2 hours at 100, 000 g at 4°C using an SW-55Ti rotor in a Beckman ultracentrifuge. After centrifugation, equal

volume of fractions were collected and loaded for western blot analysis from top layer to bottom layer. Lipid rafts and non-lipid rafts fractions were characterized by the intensity of lipid rafts markers Flotilin-1 and Gα(q). EGFR level of different fractions was quantified by ImageJ and plotted from four biological replicates.

Immunofluorescence Staining—GBM39 and HK301 cells were seeded at a density of 5×10^4 cells in laminin-coated 3.5 mm glass-bottom dishes. After 2 days, cells were washed twice with PBS and fixed in 4% PFA for 15 minutes. After fixing, cells were permeabilized with 0.2% Triton X-100 in PBS for 15 minutes and then blocked with 2% BSA in PBS for 45 minutes. Primary EGFRvIII antibody mAb806 (1:100) in PBS with 0.02% Triton X-100 and 0.5% BSA was applied to cells and incubated overnight at 4°C. After three washes with PBS, cell s were incubated with fluorescent secondary antibody Alexa Fluor anti-mouse 546 (Cat#A11018, Invitrogen) or anti-mouse 488 (Cat#A11017, Invitrogen) at a dilution of 1:1000 in PBS at room temperature for 1 hour. After four washes with PBS, the bottom glass was removed and mounted on slides with antifade reagent with DAPI (Life Technologies). Imaging was performed on an Olympus FV1000 confocal microscope.

Cell Surface EGFR and Internalization Analysis—Cell surface and internalized EGFR were measured by Flow cytometry with an EGFR antibody that recognizes the extracellular domain of both wild type EGFR and EGFRvIII as described previously (Lu et al., 2007; Luwor et al., 2001). To measure cell surface EGFR, GBM39 and HK301 cells were firstly chilled on ice for 20 minutes before incubating with a primary EGFR antibody (GR01, Millipore, mAb528, 1:20) on ice for 1 h. After gently wash by 10 ml cold PBS, the cells were then incubated on ice with an Alexa Fluor 488 goat anti mouse second antibody (Cat#A11017, Invitrogen, 1:500) for additional 1 h. After gently wash with 10 ml cold PBS, samples were analyzed on a BD LSRFortessa X-20 flow cytometer (BD Biosciences). For EGFRvIII internalization assay, U87EGFRvIII cells were cultured in medium with 1% FBS for two days and harvested for staining. Cells were firstly chilled on ice for 20 minutes and stained with the primary EGFR antibody (GR01, Millipore, mAb528, 1:40) on ice for 1 h. Primary antibody stained cells were either kept on ice or incubated at 37 ℃ for 10 minutes to allow internalization. Following internalization, the cells were washed by cold PBS and stained with Alexa Fluor 488 goat anti mouse second antibody (Cat#A11017, Invitrogen, 1:500) for another 1 h. Internalized EGFR level was defined as the decreased signal of surface EGFR after 10 minutes incubation at 37 ℃. A total of 10, 000 events for each sample was recorded and analyzed. Each experiment was repeated at least three times.

Membrane Lipid Order Analysis of GPMVs and Live Cells—Giant plasma membrane vesicles (GPMVs) were isolated and analyzed as reported previously (Sezgin et al., 2012). Briefly, normal human astrocytes (NHA) or GBM cancer cells were cultured in 6 cm dishes or 25 cm^2 flasks until nearly 70% confluency was reached. Cells were washed twice with GPMV buffer (10 mM HEPES, 150 mM NaCl, 2 mM $CaCl_2$, pH7.4) and incubated with vesiculation buffer (25mM PFA, 3 mM DTT in GPMV buffer) for 2 hours in a cell culture incubator. The supernatants were then transferred into a microcentrifuge tube and centrifuged at 100 g for 10 minutes to remove cell debris. The GPMV fraction was pelleted by centrifuging the supernatants again at 20,000 g for 1 hour at 4°C. Isolated

GPMVs were stained with 0.4 μM laurdan for 30 minutes, and the fluorescence from 400 to 550 nm was measured using the Infinite M1000 (Tecan) with excitation at 385 nm. Generalized polarization (GP) values were calculated by the formula:
$GP = (\sum_{420}^{460} Ix - \sum_{470}^{510} Ix)/(\sum_{420}^{460} Ix + \sum_{470}^{510} Ix)$.

Membrane lipid order imaging of GBM cells was performed as described previously (Owen et al., 2011). In brief, cells in glass-bottom dishes were stained with 5 μM laurdan for 3 hours in serum-free medium at 37°C in a humidified incubator with 5% CO_2, and then imaged with a Leica SP5 Confocal/Multiphoton system (excitation at 800 nm; emission at 400–460 nm and 470–530 nm). The pseudocolored GP images and HSB images were achieved using an ImageJ plug-in as described (Owen et al., 2011). HSB images that merged mean intensity and rainbow RGB color GP images were shown. GP values of thirty cells were quantified from GP images by ImageJ. Frequency of pixels with each GP value were plotted as histograms by GraphPad Prism 7 software.

Phospholipid Liposomes Preparation and Lipid Treatment—Phospholipids DPPC (PC16:0/16:0), POPC (PC16:0/18:1), and PAPC (PC16:0/20:4) (Avanti Polar Lipids) in chloroform were evaporated under a nitrogen stream and then completely dried under high vacuum. The thin lipid film was suspended in HBS buffer and incubated in 55°C water bath for 20 minutes with occasional vortexing. Lipid suspensions were then loaded into a Mini-Extruder system (Avanti Polar Lipids, Cal.610023) and passed through a 0.1 μm pore size polycarbonate membrane to generate 1 mM liposomes stocks. 10 μM of PC liposomes and equal amount of HBS buffer were used to treat cells. Media with vehicle and liposomes was refreshed every four days for soft agar colony formation assays and crystal violet clonogenic assays. 10 μM of DPPC liposomes was added to the medium one day before harvesting samples for the lipidomic analysis. For fatty acids treatment, 20 μM of fatty acids conjugated with BSA was added into growth medium supplemented with 1% FBS. Equal amount of BSA solution was added as vehicle control.

Lipidomic Analysis—All reagents were purchased from Avanti Polar Lipids except for 17:1 FFA, which was purchased from Sigma-Aldrich. shRNA lentivirus infected cells were selected with 1 μg/mL puromycin for 5 days. Cells were then reseeded in 10 cm dishes and cultured for another 3 days. Medium was changed one day before harvest. Cells were counted and washed twice with 10 mL cold DPBS, and the total cell metabolome was extracted in 4 mL 2:1:1 $CHCl_3$/MeOH/DPBS (v/v/v) solution containing the internal standard mix (500 pmol 17:1 FFA, 100 pmol 17:1 lyso-PS, 300 pmol 17:0 lyso-PC, 300 pmol 17:1 lyso-PE, 100 pmol PS(17:0/20:4), 1 nmol PC(12:0/12:0) and 1 nmol PE(12:0/12:0)). The mixture was vortexed vigorously and centrifuged at 2,000 x g for 5 minutes at 4°C. The bottom organic phase was collected, and the remaining aqueous phase was acidified with 20 μL formic acid and re-extracted by the addition of 2 mL $CHCl_3$. Both of the organic phases were pooled, dried down under N_2 gas, and reconstituted in 150 μL for LC/MS analysis. Metabolites analyzed in this study were quantified using LC/MS–based multiple reaction monitoring (MRM) methods (Agilent Technologies 6460 Triple Quad). MS analysis was performed using ESI with the following parameters: drying gas temperature, 350°C; drying gas flow, 9 l/min; nebulizer pressure, 45 Ψ; sheath gas

temperature, 375°C; sheath gas flow, 1 2 l/min; fragmentor voltage, 100 V; and capillary voltage, 3.5 kV. The separation of metabolites was achieved using a 50 mm × 4.6 mm 5 μm Gemini C18 column (Phenomenex) coupled to a guard column (Gemini: C18: 4 × 3 mm). For negative mode analysis (FFA, lyso-PS and PS measurement), H_2O: MeOH (95:5, v/v) with 0.1 % NH_4OH (v/v) and iPrOH: MeOH: H_2O (60:35:5, v/v) with 0.1 % NH_4OH (v/v) were used as buffer A and B, respectively. For positive mode analysis (lyso-PC, lyso-PE, PC and PE measurement), 20 mM ammonium acetate in H_2O and 20 mM ammonium acetate in MeOH were used as buffer A and B, respectively. The LC gradient for negative mode analysis was the following after injection: 20% B at 0.1 mL/min for 5 minutes; then increase to 85% B at 0.4 mL/min for 15 minutes; increase to 100% B at 0.5 mL/min for 5 minutes; run at 100% B at 0.5 mL/min for 2 minutes; then go back to 20% B and equilibrate at 0.5 mL/min for 5 minutes. The LC gradient for positive mode analysis was the following after injection: start from 75% B and increase to 99% B at 0.35 mL/min for 22 minutes; run at 99% B for 17 minutes; then go back to 75% B and equilibrate for 3 minutes. To determine the acyl chain composition, PC species were measured in negative ion mode using an MRM method that measures a bicarbonate adduct of PC as a parent ion and the release of an sn2 fatty acid as a product ion: $[M + HCO3]^- \rightarrow [FA - H]^-$. 5 mM ammonium bicarbonate in water and isopropanol: acetonitrile (95:5, v/v) were used as buffer A and B, respectively. The LC gradient for negative mode analysis was the following after injection: 60% B at 0.7 mL/min at 0 minute; then increase to 95% B at 0.7 mL/min for 20 minutes; stay at 95% B at 0.7 mL/min for 8 minutes, go back to 60% B at 0.7 mL/min for 2 minutes; then equilibrate at 60%B at 0.7 mL/min for 3 minutes. Lipid species were quantified by measuring areas under the curve in comparison to the corresponding internal standards using the Agilent MassHunter Quantitative Analysis Software (version B.05.00). The abundance of lipid species was then normalized to the cell numbers of each sample.

Gene Copy-number Analysis by Fluorescent *In Situ* Hybridization (FISH)— FISH analysis was performed as reported previously (Turner et al., 2017). Briefly, cells were collected, washed once with PBS and swollen with a 0.075 M KCl solution for 10 minutes. Carnoy's fixative (methanol: glacial acetic acid, 3:1) was then added dropwise to the cell suspension, centrifuged, and washed twice more with Carnoy's fixative. Cells in metaphase were then dropped onto humidified slides and aged at room temperature overnight. The fluorescent in situ hybridization (FISH) protocol was carried out by briefly immersing slides in 2X SSC buffer, followed by dehydration in 70%, 80%, and 100% ethanol solutions for 2 minutes each. To detect gene amplification, FISH probes against LPCAT1 (Cat. LPCAT1–20-RE, Empire Genomics) were applied to the dehydrated slides, a coverslip was applied, and the probe and sample were co-denatured on a 75°C heat block for 3 minutes. Slides were then placed in a 37°C humidified chamber overnight to allow hybridiz ation. Subsequently, the coverslip was removed, and slides were washed in a 0.4x SSC solution at 72°C for 2 minutes, followed by a 2 minute wash in 2x SSC containing 0.05% Tween-20. Anti-fade solution containing DAPI and a coverslip was applied to the slides. Representative cells were imaged using an Olympus BX43 microscope.

Pan-cancer Gene Copy, Expression and Patient Survival Analysis—Gene copy-number data of publically available patient datasets were obtained from cBioPortal for

Cancer Genomics (http://www.cbioportal.org/) (Cerami et al., 2012; Gao et al., 2013). TCGA provisional datasets were used for copy-number analysis. LPCAT1 expression profiles in patients across cancers were matched with TCGA normal and GTEx data, and analyzed using Gene Expression Profiling Interactive Analysis, GEPIA (Tang et al., 2017). Overall survival or disease-free survival of cancer patients in TCGA datasets with high LPCAT1 expression (top 25%) and low LPCAT1 expression (bottom 25%) was statistically compared using a Log-rank test. The cox proportional hazard ratios were also calculated, and numbers of cancer patients in each cohort were indicated in the graphs. Genomic alterations of *LPCAT1* and indicated genes in growth factor pathways across 10,967 patient samples from 33 cancer types in TCGA pan-cancer datasets were statistically analyzed by using cBioPortal.

Quantification and Statistical Analysis

Statistical Analysis: All statistical analyses were performed using GraphPad Prism 7 software. Fisher's exact test was applied for analysis of tumor tissue array. Two-tail unpaired Student's t test was used for comparing two experimental groups, and one-way or two-way ANOVA was applied when needed to compare three or more experimental groups. Log-rank (Mantel-Cox) test was used for statistical analysis of survival. We used the Shapiro-Wilk normality test to confirm that the data met assumptions of the statistical approach. Statistical tests, numbers of replicates, and p values for each experiment are indicated in the figure legends or methods.

Supplementary Material

Refer to Web version on PubMed Central for supplementary material.

Acknowledgments

This work was supported by the Ludwig Institute for Cancer Research and grants from National Institute for Neurological Diseases and Stroke (NS73831), the Defeat GBM Program of the National Brain Tumor Society, the Ben and Catherine Ivy Foundation, an award from the Sharpe/National Brain Tumor Society Research Program, and a Compute for the Cure Award from the Nvidia Foundation (P.S.M.), as well as the UCSD Neuroscience Microscopy Shared Facility Grant (P30 NS047101).

References

Abdelzaher E, and Mostafa MF (2015). Lysophosphatidylcholine acyltransferase 1 (LPCAT1) upregulation in breast carcinoma contributes to tumor progression and predicts early tumor recurrence. Tumour biology : the journal of the International Society for Oncodevelopmental Biology and Medicine 36, 5473–5483. [PubMed: 25683484]

Abercrombie M, and Ambrose EJ (1962). The surface properties of cancer cells: a review. Cancer research 22, 525–548. [PubMed: 13858936]

Arkhipov A, Shan Y, Das R, Endres NF, Eastwood MP, Wemmer DE, Kuriyan J, and Shaw DE (2013). Architecture and membrane interactions of the EGF receptor. Cell 152, 557–569. [PubMed: 23374350]

Bridges JP, Ikegami M, Brilli LL, Chen X, Mason RJ, and Shannon JM (2010). LPCAT1 regulates surfactant phospholipid synthesis and is required for transitioning to air breathing in mice. The Journal of clinical investigation 120, 1736–1748. [PubMed: 20407208]

Cerami E, Gao J, Dogrusoz U, Gross BE, Sumer SO, Aksoy BA, Jacobsen A, Byrne CJ, Heuer ML, Larsson E, et al. (2012). The cBio cancer genomics portal: an open platform for exploring multidimensional cancer genomics data. Cancer discovery 2, 401–404. [PubMed: 22588877]

Cizmecioglu O, Ni J, Xie S, Zhao JJ, and Roberts TM (2016). Rac1-mediated membrane raft localization of PI3K/p110beta is required for its activation by GPCRs or PTEN loss. eLife 5.

Cloughesy TF, Cavenee WK, and Mischel PS (2014). Glioblastoma: from molecular pathology to targeted treatment. Annual review of pathology 9, 1–25.

Cotte AK, Aires V, Fredon M, Limagne E, Derangere V, Thibaudin M, Humblin E, Scagliarini A, de Barros JP, Hillon P, et al. (2018). Lysophosphatidylcholine acyltransferase 2-mediated lipid droplet production supports colorectal cancer chemoresistance. Nature communications 9, 322.

Currie E, Schulze A, Zechner R, Walther TC, and Farese RV Jr. (2013). Cellular fatty acid metabolism and cancer. Cell metabolism 18, 153–161. [PubMed: 23791484]

Du Y, Wang Q, Zhang X, Wang X, Qin C, Sheng Z, Yin H, Jiang C, Li J, and Xu T (2017). Lysophosphatidylcholine acyltransferase 1 upregulation and concomitant phospholipid alterations in clear cell renal cell carcinoma. Journal of experimental & clinical cancer research : CR 36, 66. [PubMed: 28494778]

Friedman JS, Chang B, Krauth DS, Lopez I, Waseem NH, Hurd RE, Feathers KL, Branham KE, Shaw M, Thomas GE, et al. (2010). Loss of lysophosphatidylcholine acyltransferase 1 leads to photoreceptor degeneration in rd11 mice. Proceedings of the National Academy of Sciences of the United States of America 107, 15523–15528. [PubMed: 20713727]

Gao J, Aksoy BA, Dogrusoz U, Dresdner G, Gross B, Sumer SO, Sun Y, Jacobsen A, Sinha R, Larsson E, et al. (2013). Integrative analysis of complex cancer genomics and clinical profiles using the cBioPortal. Science signaling 6, pl1. [PubMed: 23550210]

Guo D, Prins RM, Dang J, Kuga D, Iwanami A, Soto H, Lin KY, Huang TT, Akhavan D, Hock MB, et al. (2009). EGFR signaling through an Akt-SREBP-1-dependent, rapamycin-resistant pathway sensitizes glioblastomas to antilipogenic therapy. Science signaling 2, ra82.

Guo D, Reinitz F, Youssef M, Hong C, Nathanson D, Akhavan D, Kuga D, Amzajerdi AN, Soto H, Zhu S, et al. (2011). An LXR agonist promotes glioblastoma cell death through inhibition of an EGFR/AKT/SREBP-1/LDLR-dependent pathway. Cancer discovery 1, 442–456. [PubMed: 22059152]

Guri Y, Colombi M, Dazert E, Hindupur SK, Roszik J, Moes S, Jenoe P, Heim MH, Riezman I, Riezman H, et al. (2017). mTORC2 Promotes Tumorigenesis via Lipid Synthesis. Cancer cell 32, 807–823 e812. [PubMed: 29232555]

Hanahan D, and Weinberg RA (2011). Hallmarks of cancer: the next generation. Cell 144, 646–674. [PubMed: 21376230]

Harayama T, Eto M, Shindou H, Kita Y, Otsubo E, Hishikawa D, Ishii S, Sakimura K, Mishina M, and Shimizu T (2014). Lysophospholipid acyltransferases mediate phosphatidylcholine diversification to achieve the physical properties required in vivo. Cell metabolism 20, 295–305. [PubMed: 24981836]

Harayama T, and Riezman H (2018). Understanding the diversity of membrane lipid composition. Nature reviews Molecular cell biology 19, 281–296. [PubMed: 29410529]

Hashidate-Yoshida T, Harayama T, Hishikawa D, Morimoto R, Hamano F, Tokuoka SM, Eto M, Tamura-Nakano M, Yanobu-Takanashi R, Mukumoto Y, et al. (2015). Fatty acid remodeling by LPCAT3 enriches arachidonate in phospholipid membranes and regulates triglyceride transport. eLife 4.

Hilvo M, Denkert C, Lehtinen L, Muller B, Brockmoller S, Seppanen-Laakso T, Budczies J, Bucher E, Yetukuri L, Castillo S, et al. (2011). Novel theranostic opportunities offered by characterization of altered membrane lipid metabolism in breast cancer progression. Cancer research 71, 3236–3245. [PubMed: 21415164]

Hishikawa D, Hashidate T, Shimizu T, and Shindou H (2014). Diversity and function of membrane glycerophospholipids generated by the remodeling pathway in mammalian cells. Journal of lipid research 55, 799–807. [PubMed: 24646950]

Hishikawa D, Shindou H, Kobayashi S, Nakanishi H, Taguchi R, and Shimizu T (2008). Discovery of a lysophospholipid acyltransferase family essential for membrane asymmetry and diversity.

Proceedings of the National Academy of Sciences of the United States of America 105, 2830–2835. [PubMed: 18287005]

Kurabe N, Hayasaka T, Ogawa M, Masaki N, Ide Y, Waki M, Nakamura T, Kurachi K, Kahyo T, Shinmura K, et al. (2013). Accumulated phosphatidylcholine (16:0/16:1) in human colorectal cancer; possible involvement of LPCAT4. Cancer science 104, 1295–1302. [PubMed: 23815430]

Lands WE (1958). Metabolism of glycerolipides; a comparison of lecithin and triglyceride synthesis. The Journal of biological chemistry 231, 883–888. [PubMed: 13539023]

Lingwood D, and Simons K (2010). Lipid rafts as a membrane-organizing principle. Science 327, 46–50. [PubMed: 20044567]

Lu Y, Li X, Liang K, Luwor R, Siddik ZH, Mills GB, Mendelsohn J, and Fan Z (2007). Epidermal growth factor receptor (EGFR) ubiquitination as a mechanism of acquired resistance escaping treatment by the anti-EGFR monoclonal antibody cetuximab. Cancer research 67, 8240–8247. [PubMed: 17804738]

Luwor RB, Johns TG, Murone C, Huang HJ, Cavenee WK, Ritter G, Old LJ, Burgess AW, and Scott AM (2001). Monoclonal antibody 806 inhibits the growth of tumor xenografts expressing either the de2–7 or amplified epidermal growth factor receptor (EGFR) but not wild-type EGFR. Cancer research 61, 5355–5361. [PubMed: 11454674]

Ma PC, Jagadeeswaran R, Jagadeesh S, Tretiakova MS, Nallasura V, Fox EA, Hansen M, Schaefer E, Naoki K, Lader A, et al. (2005). Functional expression and mutations of c-Met and its therapeutic inhibition with SU11274 and small interfering RNA in non-small cell lung cancer. Cancer research 65, 1479–1488. [PubMed: 15735036]

Ma PC, Kijima T, Maulik G, Fox EA, Sattler M, Griffin JD, Johnson BE, and Salgia R (2003). c-MET mutational analysis in small cell lung cancer: novel juxtamembrane domain mutations regulating cytoskeletal functions. Cancer research 63, 6272–6281. [PubMed: 14559814]

Macdonald JL, and Pike LJ (2005). A simplified method for the preparation of detergent-free lipid rafts. Journal of lipid research 46, 1061–1067. [PubMed: 15722565]

Mansilla F, da Costa KA, Wang S, Kruhoffer M, Lewin TM, Orntoft TF, Coleman RA, and Birkenkamp-Demtroder K (2009). Lysophosphatidylcholine acyltransferase 1 (LPCAT1) overexpression in human colorectal cancer. Journal of molecular medicine 87, 85–97. [PubMed: 18974965]

Morita Y, Sakaguchi T, Ikegami K, Goto-Inoue N, Hayasaka T, Hang VT, Tanaka H, Harada T, Shibasaki Y, Suzuki A, et al. (2013). Lysophosphatidylcholine acyltransferase 1 altered phospholipid composition and regulated hepatoma progression. Journal of hepatology 59, 292–299. [PubMed: 23567080]

Nakanishi H, Shindou H, Hishikawa D, Harayama T, Ogasawara R, Suwabe A, Taguchi R, and Shimizu T (2006). Cloning and characterization of mouse lung-type acyl-CoA:lysophosphatidylcholine acyltransferase 1 (LPCAT1). Expression in alveolar type II cells and possible involvement in surfactant production. The Journal of biological chemistry 281, 20140–20147. [PubMed: 16704971]

Nathanson DA, Gini B, Mottahedeh J, Visnyei K, Koga T, Gomez G, Eskin A, Hwang K, Wang J, Masui K, et al. (2014). Targeted therapy resistance mediated by dynamic regulation of extrachromosomal mutant EGFR DNA. Science 343, 72–76. [PubMed: 24310612]

Nomura DK, Long JZ, Niessen S, Hoover HS, Ng SW, and Cravatt BF (2010). Monoacylglycerol lipase regulates a fatty acid network that promotes cancer pathogenesis. Cell 140, 49–61. [PubMed: 20079333]

Ogretmen B (2018). Sphingolipid metabolism in cancer signalling and therapy. Nature reviews Cancer 18, 33–50. [PubMed: 29147025]

Owen DM, Rentero C, Magenau A, Abu-Siniyeh A, and Gaus K (2011). Quantitative imaging of membrane lipid order in cells and organisms. Nature protocols 7, 24–35. [PubMed: 22157973]

Parasassi T, Gratton E, Yu WM, Wilson P, and Levi M (1997). Two-photon fluorescence microscopy of laurdan generalized polarization domains in model and natural membranes. Biophysical journal 72, 2413–2429. [PubMed: 9168019]

Pavlova NN, and Thompson CB (2016). The Emerging Hallmarks of Cancer Metabolism. Cell metabolism 23, 27–47. [PubMed: 26771115]

Pike LJ, Han X, and Gross RW (2005). Epidermal growth factor receptors are localized to lipid rafts that contain a balance of inner and outer leaflet lipids: a shotgun lipidomics study. The Journal of biological chemistry 280, 26796–26804. [PubMed: 15917253]

Pinot M, Vanni S, Pagnotta S, Lacas-Gervais S, Payet LA, Ferreira T, Gautier R, Goud B, Antonny B, and Barelli H (2014). Polyunsaturated phospholipids facilitate membrane deformation and fission by endocytic proteins. Science 345, 693–697. [PubMed: 25104391]

Rajendran L, and Simons K (2005). Lipid rafts and membrane dynamics. Journal of cell science 118, 1099–1102. [PubMed: 15764592]

Rohrig F, and Schulze A (2016). The multifaceted roles of fatty acid synthesis in cancer. Nature reviews Cancer 16, 732–749. [PubMed: 27658529]

Rysman E, Brusselmans K, Scheys K, Timmermans L, Derua R, Munck S, Van Veldhoven PP, Waltregny D, Daniels VW, Machiels J, et al. (2010). De novo lipogenesis protects cancer cells from free radicals and chemotherapeutics by promoting membrane lipid saturation. Cancer research 70, 8117–8126. [PubMed: 20876798]

Sanchez-Vega F, Mina M, Armenia J, Chatila WK, Luna A, La KC, Dimitriadoy S, Liu DL, Kantheti HS, Saghafinia S, et al. (2018). Oncogenic Signaling Pathways in The Cancer Genome Atlas. Cell 173, 321–337 e310. [PubMed: 29625050]

Sezgin E, Kaiser HJ, Baumgart T, Schwille P, Simons K, and Levental I (2012). Elucidating membrane structure and protein behavior using giant plasma membrane vesicles. Nature protocols 7, 1042–1051. [PubMed: 22555243]

Sezgin E, Levental I, Mayor S, and Eggeling C (2017). The mystery of membrane organization: composition, regulation and roles of lipid rafts. Nature reviews Molecular cell biology 18, 361–374. [PubMed: 28356571]

Shannon P, Markiel A, Ozier O, Baliga NS, Wang JT, Ramage D, Amin N, Schwikowski B, and Ideker T (2003). Cytoscape: a software environment for integrated models of biomolecular interaction networks. Genome research 13, 2498–2504. [PubMed: 14597658]

Shida-Sakazume T, Endo-Sakamoto Y, Unozawa M, Fukumoto C, Shimada K, Kasamatsu A, Ogawara K, Yokoe H, Shiiba M, Tanzawa H, et al. (2015). Lysophosphatidylcholine acyltransferase1 overexpression promotes oral squamous cell carcinoma progression via enhanced biosynthesis of platelet-activating factor. PloS one 10, e0120143. [PubMed: 25803864]

Tang Z, Li C, Kang B, Gao G, Li C, and Zhang Z (2017). GEPIA: a web server for cancer and normal gene expression profiling and interactive analyses. Nucleic acids research 45, W98–W102. [PubMed: 28407145]

Tomas A, Futter CE, and Eden ER (2014). EGF receptor trafficking: consequences for signaling and cancer. Trends in cell biology 24, 26–34. [PubMed: 24295852]

Turner KM, Deshpande V, Beyter D, Koga T, Rusert J, Lee C, Li B, Arden K, Ren B, Nathanson DA, et al. (2017). Extrachromosomal oncogene amplification drives tumour evolution and genetic heterogeneity. Nature 543, 122–125. [PubMed: 28178237]

Uehara T, Kikuchi H, Miyazaki S, Iino I, Setoguchi T, Hiramatsu Y, Ohta M, Kamiya K, Morita Y, Tanaka H, et al. (2016). Overexpression of Lysophosphatidylcholine Acyltransferase 1 and Concomitant Lipid Alterations in Gastric Cancer. Annals of surgical oncology 23 Suppl 2, S206–213. [PubMed: 25752890]

van Meer G, Voelker DR, and Feigenson GW (2008). Membrane lipids: where they are and how they behave. Nature reviews Molecular cell biology 9, 112–124. [PubMed: 18216768]

Villa GR, Hulce JJ, Zanca C, Bi J, Ikegami S, Cahill GL, Gu Y, Lum KM, Masui K, Yang H, et al. (2016). An LXR-Cholesterol Axis Creates a Metabolic Co-Dependency for Brain Cancers. Cancer cell 30, 683–693. [PubMed: 27746144]

Wang B, Rong X, Duerr MA, Hermanson DJ, Hedde PN, Wong JS, Vallim TQ, Cravatt BF, Gratton E, Ford DA, et al. (2016). Intestinal Phospholipid Remodeling Is Required for Dietary-Lipid Uptake and Survival on a High-Fat Diet. Cell metabolism 23, 492–504. [PubMed: 26833026]

Wang B, Rong X, Palladino END, Wang J, Fogelman AM, Martin MG, Alrefai WA, Ford DA, and Tontonoz P (2018). Phospholipid Remodeling and Cholesterol Availability Regulate Intestinal Stemness and Tumorigenesis. Cell stem cell 22, 206–220 e204. [PubMed: 29395055]

Wang MY, Lu KV, Zhu S, Dia EQ, Vivanco I, Shackleford GM, Cavenee WK, Mellinghoff IK, Cloughesy TF, Sawyers CL, et al. (2006). Mammalian target of rapamycin inhibition promotes response to epidermal growth factor receptor kinase inhibitors in PTEN-deficient and PTEN-intact glioblastoma cells. Cancer research 66, 7864–7869. [PubMed: 16912159]

Wang Y, Gao J, Guo X, Tong T, Shi X, Li L, Qi M, Wang Y, Cai M, Jiang J, et al. (2014). Regulation of EGFR nanocluster formation by ionic protein-lipid interaction. Cell research 24, 959–976. [PubMed: 25001389]

Zhou Y, Prakash P, Liang H, Cho KJ, Gorfe AA, and Hancock JF (2017). Lipid-Sorting Specificity Encoded in K-Ras Membrane Anchor Regulates Signal Output. Cell 168, 239–251 e216. [PubMed: 28041850]

Zwang Y, and Yarden Y (2006). p38 MAP kinase mediates stress-induced internalization of EGFR: implications for cancer chemotherapy. The EMBO journal 25, 4195–4206. [PubMed: 16932740]

Highlights

- Persistent EGFR signaling activates membrane lipid remodeling through LPCAT1
- LPCAT1 regulates phospholipid saturation and oncogenic growth factor signaling
- *LPCAT1* is frequently amplified in cancer and associated with poor patient survival
- Membrane phospholipid remodeling generates an actionable dependency across cancers

Context and Significance

Cancer is a process of unrestrained cell division. Receptors on the surface of cells frequently become genetically altered, existing as ‘oncogenic receptors’ and sending signals that drive unrestrained cell division, leading to tumor formation and cancer progression. A team of researchers in San Diego discovered that an enzyme that controls specific lipid properties of the cell membrane is required for oncogenic receptors to properly localize on the cell surface. Targeting this enzyme caused oncogenic growth factor receptors to dissociate from the cell membrane, blocking their signaling and inducing massive tumor cell death, with greatly increased survival in mice bearing a variety of different cancers. The study highlights an important link between cancer causing genes (oncogenes) and membrane lipids, suggesting a compelling new cancer drug target.

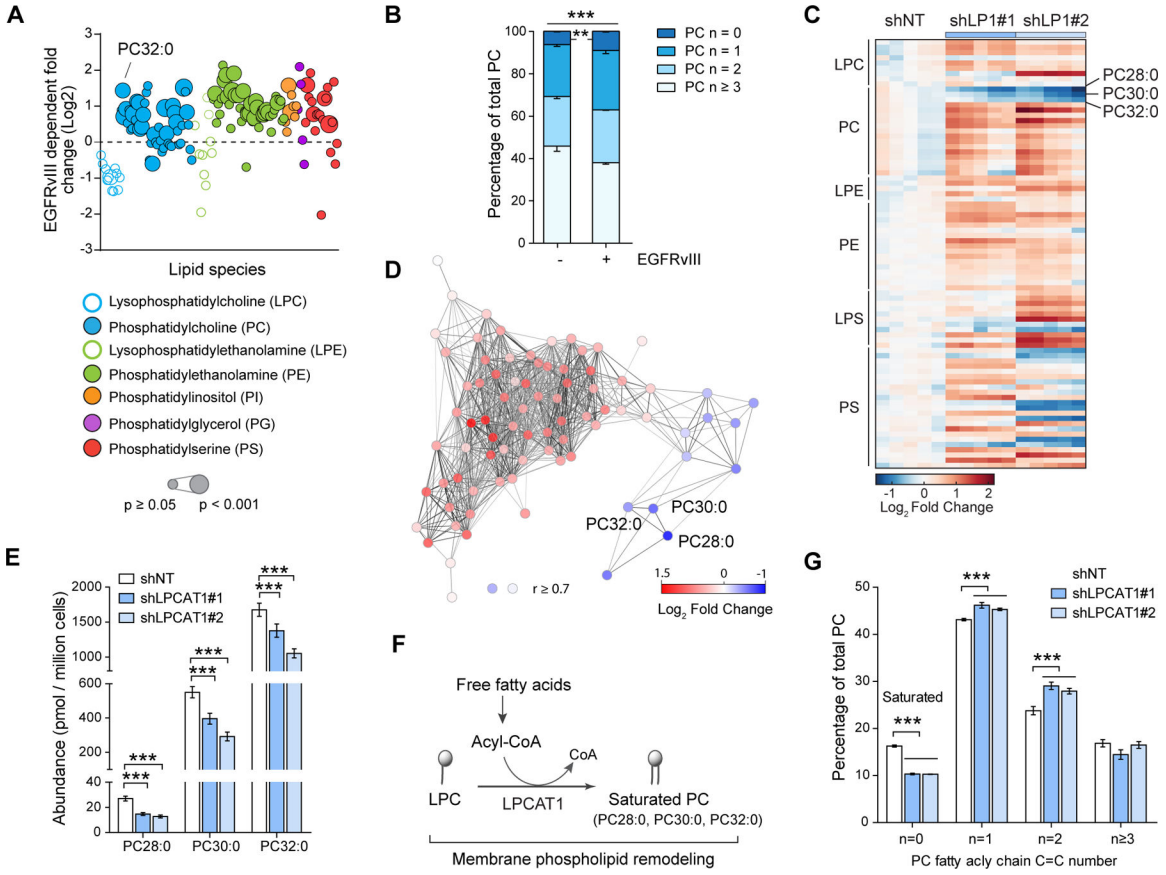

Figure 1. EGFRvIII Signaling Activates Membrane Phospholipid Remodeling of Cancer Cells through LPCAT1

(A) Lipidomics analysis of phospholipids in U87EGFRvIII and U87 cells. Values are shown as log2 fold change relative to U87 cells. Each dot represents one lipid species. Dot color shows lipid class and dot size indicates significance.

(B) Percentage of phosphatidylcholine (PC) with different saturation indexes in U87EGFRvIII and U87 cells. Saturation index (n) of PC was calculated by the total numbers of carbon double bonds contained in two fatty acyl chains. n = 0 represents saturated PC.

(C) Heatmap of phospholipid changes in U87EGFRvIII cells expressing non-targeting control and LPCAT1 shRNA. Color Scale represents log2 fold change of lipid abundance relative to shNT control. Five replicates for each group were performed. Three saturated PCs, PC28:0, PC30:0 and PC32:0 are labeled.

(D) Lipid-lipid interaction network in EGFRvIII-expressing cancer cells. Pearson's correlations between pairs of lipids were calculated based on their relative abundance over fifteen independent experiments of (C) and represented by edge darkness. Edges with r >= 0.7 are visualized. Node color represents log2 fold change of lipid abundance relative to control. The network is visualized in Cytoscape (Shannon et al., 2003).

(E) The abundance (pmol/ million cells) of three saturated phosphatidylcholine PC28:0, PC30:0 and PC32:0 in U87EGFRvIII cells expressing control and LPCAT1 shRNA. Data represent mean SEM.

(F) Schematic model for LPCAT1 function in phospholipid remodeling converting lysophosphatidylcholine (LPC) to saturated PC, including PC28:0, PC30:0 and PC32:0, in cancer cells.

(G) Percentage of phosphatidylcholine with different saturation indexes in total PC. The saturation index of PC was calculated by the total numbers of carbon double bonds contained in two fatty acyl chains. Data represent mean ± SD.

Statistical analysis was performed with student's t test for (A), and one-way ANOVA plus a Tukey's multiple comparisons test for (B), and two-way ANOVA plus a Dunnett's multiple comparisons test for (E) and (G). ***$p < 0.001$, **$p < 0.01$.

See also Figure S1 and Table S1.

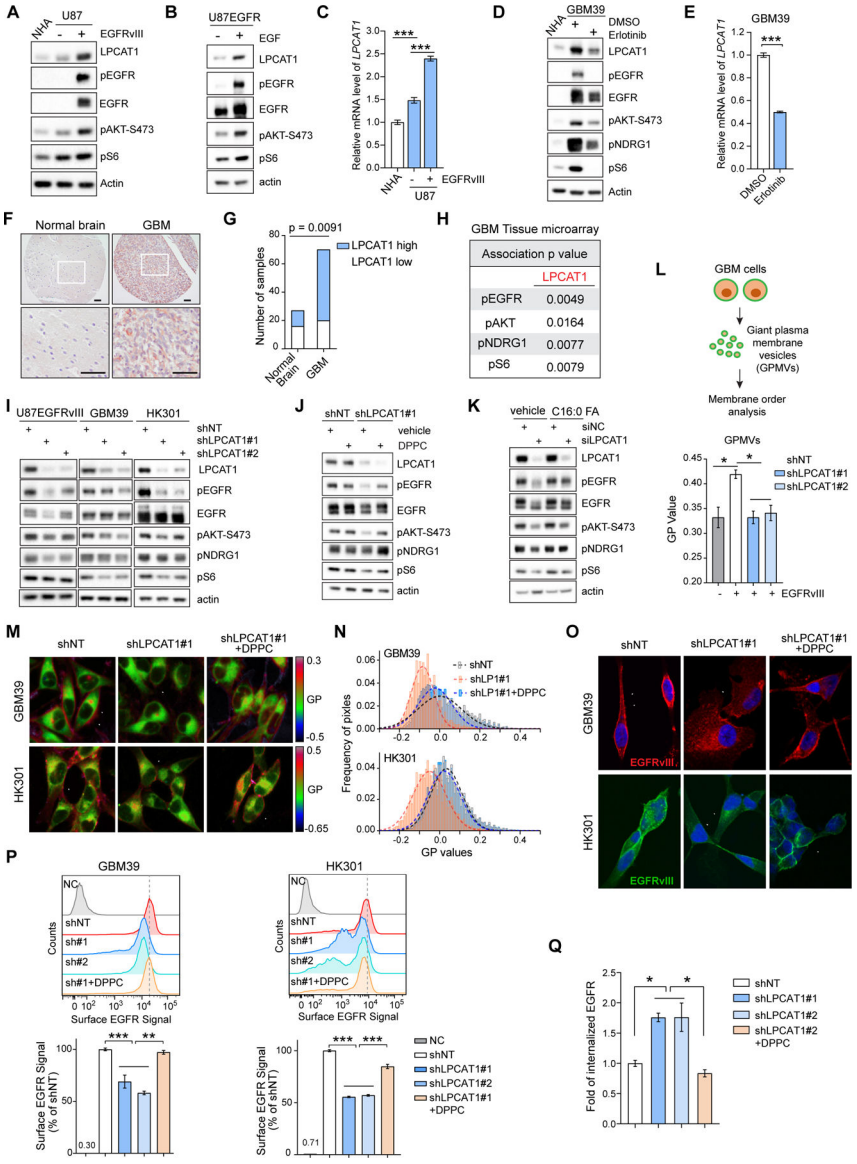

Figure 2. LPCAT1 Is Highly Upregulated in EGFR-activated GBM Samples, and Is Required for EGFR Signaling

(A) Western blot analysis of LPCAT1 expression and EGFR signaling in normal human astrocytes (NHA), U87 and U87EGFRvIII cells.

(B) Western blot analysis of LPCAT1 expression and EGFR signaling in U87cells expressing EGFR with or without EGF (20 ng/ml) stimulation for 24 hours.

(C) Relative mRNA level of LPCAT1 in normal human astrocytes (NHA), U87 and U87EGFRvIII cells. Data represent mean ± SD.

(D) Western blot analysis of LPCAT1 expression and EGFR signaling in normal human astrocytes (NHA) and patient-derived neurosphere GBM39 cells treated with DMSO or erlotinib (10 μM) for 48 hours. Erlotinib is an inhibitor to block EGFR signaling.

(E) Relative mRNA level of LPCAT1 in GBM39 cells treated with DMSO or erlotinib (10 μM) for 48 hours. Data represent mean ± SD.

(F) Representative images of immunohistochemistry (IHC) staining for LPCAT1 in GBM patient tumor samples (n =70) and adjacent normal brain tissue cores (n = 27) and. Scale bar, 50 μm.
(G) Quantification of LPCAT1 IHC staining in GBM tissue microarray samples. Numbers of samples with LPCAT1 high or low staining intensity are shown.
(H) LPCAT1 protein level is correlated with EGFR signaling in GBM patient samples. Intensity of IHC staining for indicated proteins was scored and quantified.
(I) Western blot analysis of EGFR signaling in U87EGFRvIII, GBM39 and HK301 cells expressing control and LPCAT1 shRNA.
(J) Western blot analysis of EGFR signaling in U87EGFRvIII cells expressing control and LPCAT1 shRNA. Cells were treated with vehicle control or 10 M of DPPC (PC16:0/16:0) liposomes.
(K) Western blot analysis of EGFR signaling in U87EGFRvIII cells transfected with negative control and LPCAT1 siRNA. Cells were treated with vehicle control or 20 M of palmitate (C16:0 FA).
(L) Membrane order changes of giant plasma membrane vesicles (GPMVs) isolated from U87 cells or U87EGFRvIII cells expressing control or LPCAT1shRNA. General polarization (GP) values were determined by laurdan staining. Data represent mean SEM.
(M) Laurdan imaging analysis of membrane lipid order in GBM39 and HK301 cells expressing control and LPCAT1 shRNA. 10 M of DPPC liposomes was added to rescue membrane order after LPCAT1 depletion. Merged mean intensity and rainbow RGB pseudocolored GP images are shown. Red colors indicate high membrane order and less membrane dynamic, whereas blue colors indicate low order and high membrane dynamic. Arrowheads point to plasma membrane. Scale bar, 20 μm.
(N) Distribution of the GP values in GBM39 and HK301 cells in (M). The histograms for GBM cells with LPCAT1 knockdown are shifted to low GP values.
(O) Immunofluorescence staining of EGFRvIII in GBM39 and HK301 cells expressing control and LPCAT1 shRNA. 10 M of DPPC liposomes was added to rescue EGFRvIII localization after LPCAT1 depletion. Arrowheads point to plasma membrane staining of EGFRvIII. Nuclei were stained with DAPI (blue). Scale bar, 20 μm.
(P) Flow cytometry analysis of cell surface EGFR in GBM39 and HK301 cells with indicated treatment. 10 M of DPPC liposomes was added after LPCAT1 depletion in rescue groups. Cells only stained with secondary antibody were performed as the negative control (NC). Data represent mean SEM.
(Q) Fold change of internalized surface EGFR in U87EGFRvIII cells expressing control and LPCAT1 shRNA after 10-minutes internalization at 37 ?. Data represent mean SEM. 10 M of DPPC liposomes was added after LPCAT1 depletion in the rescue group.
Statistical analysis was performed with Fisher's exact test for (G) and (H), and Student's t test for (C), (E), (L) (P) and (Q). ***$p < 0.001$, **$p < 0.01$;*$p < 0.05$.
See also Figure S2.

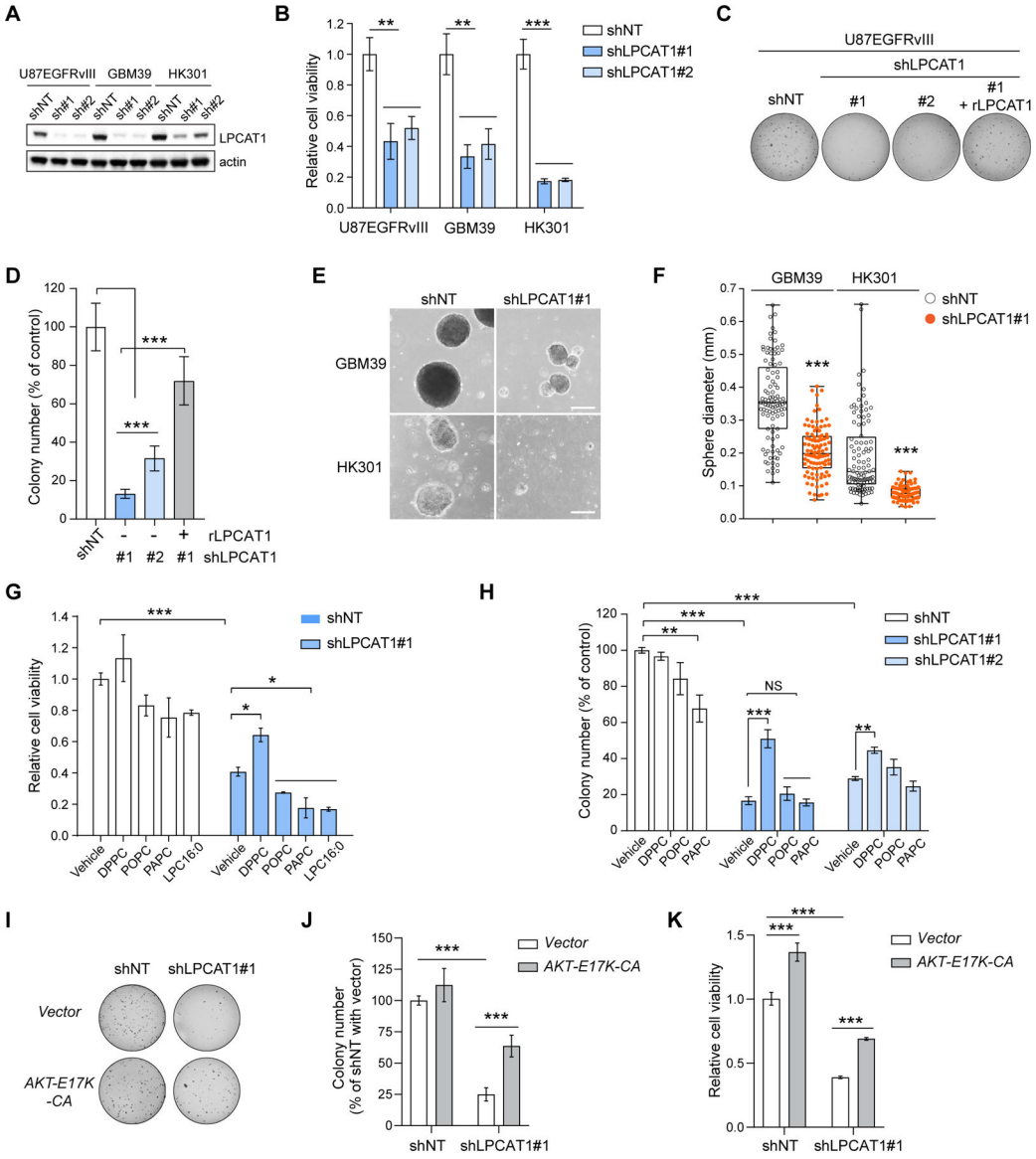

Figure 3. LPCAT1-mediated Phospholipid Saturation Promotes Cancer Cell Proliferation and Survival

(A) Knockdown efficiency of LPCAT1 shRNAs in three GBM cancer cell lines.

(B) Relative cell viability of U87EGFRvIII, GBM39 and HK301 cells expressing control and LPCAT1 shRNA.

(C) Colony formation assay was performed in soft agar for U87EGFRvIII cells expressing control and LPCAT1 shRNA. A shRNA-resistant form of LPCAT1 was expressed in cancer cells with #1 shRNA.

(D) Quantification of colony numbers in (C).

(E) Representative sphere images of two patient-derived neurosphere lines GBM39 and HK301 expressing control and LPCAT1 shRNA. Scale bar, 250 μm.

(F) Quantification of sphere diameters of (E). The median value (center line), the min and max (whiskers), and the 25th and 75th percentiles (box perimeters) are presented. Each dot represents one sphere.

(G) Relative cell viability of LPCAT1 knockdown and control U87EGFRvIII cells with 10 M indicated lipids or vehicle treatments. Liposomes of indicated PCs were generated and treated to cells. DPPC, PC16:0/16:0; POPC, PC16:0/18:1; PAPC, PC16:0/20:4.
(H) Colony formation assay was performed in soft agar for U87EGFRvIII cell expressing control and LPCAT1 shRNA with 10 M of lipids or vehicle treatments. Liposomes of indicated PCs were generated and treated to cells.
(I-J) Colony formation assay was performed in soft agar for U87EGFRvIII cells expressing indicated shRNA or vectors. An empty vector or a vector expressing a constitutively active form of AKT with E17K mutation was stably transfected into the indicated cells.
(K) Relative cell viability of U87EGFRvIII cells expressing indicated shRNA or vectors. Data represent mean ± SD except (F). Statistical analysis was performed with one-way ANOVA for (B), (F), (J) and (K), two-way ANOVA plus a Tukey's multiple comparisons test for (G) and (H), and Student's t test for (D). ***$p < 0.001$, **$p < 0.01$, *$p < 0.05$, NS, not significant.
See also Figure S3.

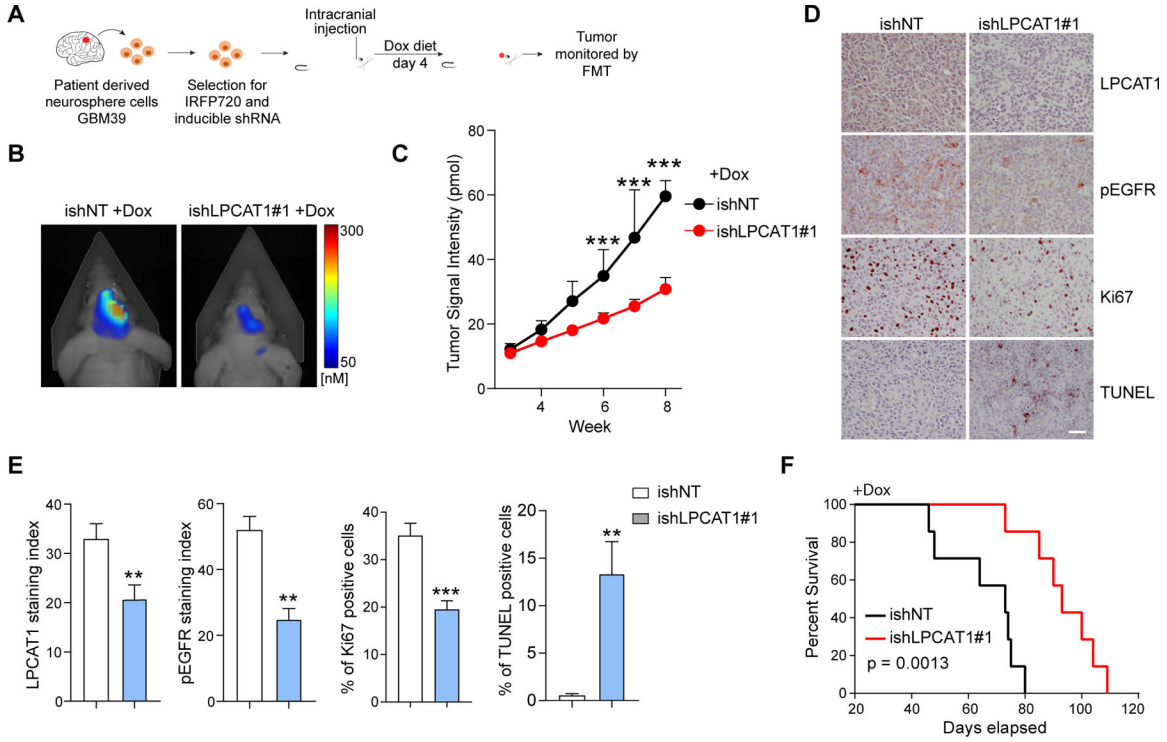

Figure 4. LPCAT1 Depletion Suppresses Tumor Growth and Prolongs the Survival of Mice Bearing Intracranial Patient-Derived GBMs

(A). Schematic of genetic depletion of LPCAT1 in the patient-derived GBM orthotopic xenograft model using doxycycline-inducible shRNA. Patient-derived neurosphere GBM39 cells, engineered to carry for both near-infrared fluorescent protein 720 (IRFP 720) and inducible shRNA, were orthotopically injected into five-week old nu/nu mice (n=7 for each group). Dox diet was given at day 4 after injection.

(B) Representative FMT tumor images of mice at week 8 after injection shows inducible knockdown of LPCAT1 suppresses GBM tumor growth. Scale bar, 3.8 mm.

(C) Tumor growth curves for mice bearing GBM with inducible expression of non-targeting control or LPCAT1 shRNA. Error bars represent ± SD.

(D) IHC staining of tumor samples of (C) with indicated antibodies. Scale bar, 50 μm.

(E) Quantification of the IHC staining in (D).

(F) Kaplan-Meier curves for the overall survival of mice from (C). p = 0.0013.

Data represent mean ± SD. Statistical analysis was performed with Student's t test for (E), Two-way ANOVA with a post Tukey's multiple comparisons test for (C), and Log-rank test for (F). ***p < 0.001, **p < 0.01.

See also Figure S4.

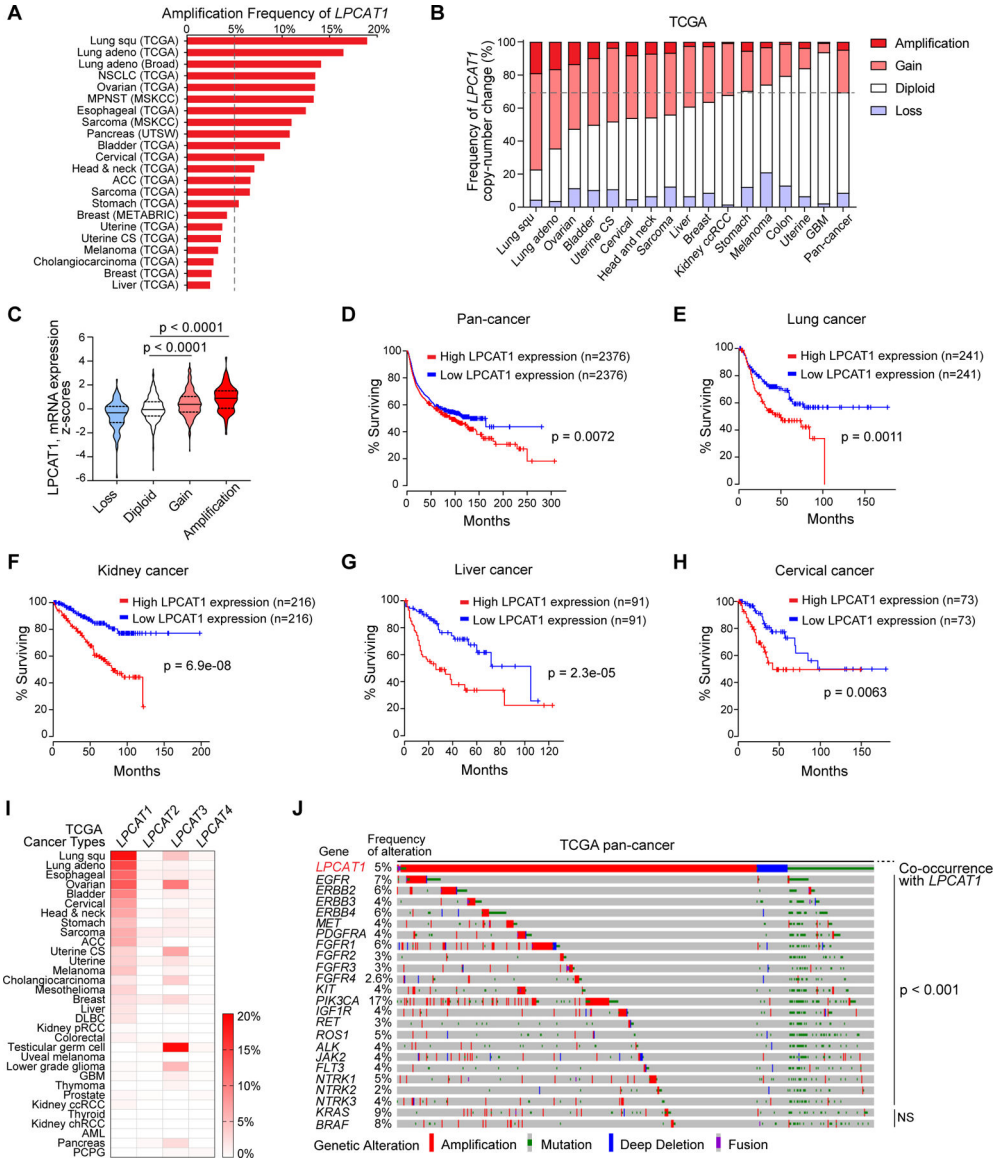

Figure 5. *LPCAT1* Is Frequently Amplified and Associated with Shorter Patient Survival in Cancer

(A) Amplification frequency of *LPCAT1* across cancers in publically available cancer sequencing databases of clinical samples. Cancer types with over 2.5% amplification are shown.

(B) Copy-number alternations of *LPCAT1* across cancers in TCGA datasets. *LPCAT1* copy number is increased in over 30% of pan-cancer patients.

(C) Violin plots of LPCAT1 mRNA expression (z-scores) versus copy numbers in Cancer Cell Line Encyclopedia (CCLE) cell lines. The median value (center line) and the 25th and 75th percentiles (dash lines) are presented.

(D-E) The disease-free survival of patients with high or low LPCAT1 expression in pan-cancer (D) and pan-lung cancer (E) from TCGA cancer data sets. The high or low LPCAT1 expression was defined as a value in the top quartile or bottom quartile of the set, respectively.

(F-H) The overall survival of patients with high or low LPCAT1 expression in kidney cancer, liver cancer and cervical cancer from TCGA cancer data sets. The high or low LPCAT1 expression was defined as in (D-E).

(I) Heatmap of gene amplification frequency of *LPCAT1–4* in TCGA cancer datasets.

(J) Genomic alternations of *LPCAT1* and genes in growth factor pathways in TCGA pan-cancer datasets. Indicated gene alternations across 10,967 patient samples from 33 cancer types in TCGA pan-cancer datasets were analyzed by using cBioPortal. Only patient samples with genomic alternations in *LPCAT1* were visualized.

Statistical analysis was performed with one-way ANOVA plus a post Tukey's multiple comparisons test for (C), Log-rank test for (D-H), and Fisher's exact test for (J).

See also Figure S5 and Table S2.

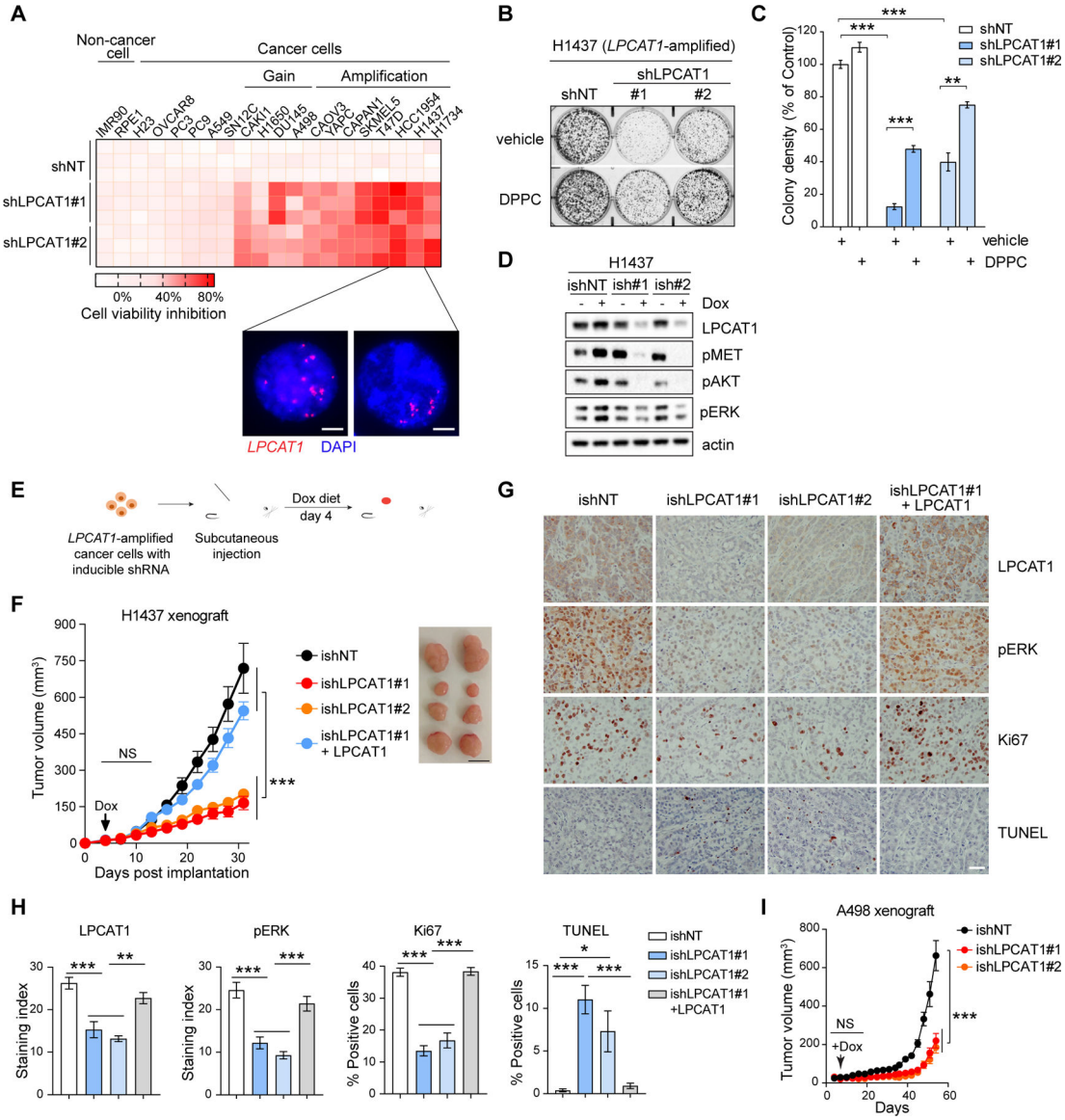

Figure 6. LPCAT1 Depletion Effectively Kills a Wide Variety of *LPCAT1* Copy-number Increased Cancers via Its Effect on Saturated PC Synthesis

(A) Cell viability of 2 non-cancer cell lines and 18 cancer cell lines expressing control and LPCAT1 shRNA. Cell viability data was normalized with control. *LPCAT1* copy number of two representative cancer cell lines (H1437 and HCC1954) with *LPCAT1*-amplification was validated by FISH with a *LPCAT1*-specific probe (red). Nuclear DNA was counterstained with DAPI (blue). Scale bar, 5 μm.

(B) Colony formation of control and LPCAT1 knockdown H1437 cells treated with vehicle or 10 M of DPPC liposomes.

(C) Quantification of colony density in (B). Percentage of colony density relative to control cells with vehicle treatment are shown. Error bars represent ± SD.

(D) Western blot analysis of H1437 cells expressing doxycycline-induced shRNAs with indicated antibodies.

(E) Schematic of genetic depletion of LPCAT1 in *LPCAT1*-amplified cancer models using doxycycline-inducible shRNA system. LPCAT1-amplified cancer cell lines, engineered to carry inducible shRNA, were subcutaneously injected into five-week old nu/nu mice (n=8 for each group). Dox diet was given after tumors were established at day 4 after implantation.

(F) Tumor growth of mice carrying *LPCAT1*-amplified lung cancer cell H1437 xenografts expressing non-targeting or LPCAT1-targeting inducible shRNA. Flag-tagged LPCAT1 was expressed in the rescue group with LPCAT1#1 inducible shRNA that targets to 3'UTR region of *LPCAT1*. Error bars represent SEM. Two representative tumor images for each group are shown. Scale bar, 10 mm.

(G) IHC staining of H1437 xenograft tumor samples with indicated antibodies. Scale bar, 50 μm.

(H) Quantification of the IHC staining in (G). Data represent mean ± SD.

(I) Tumor growth of mice subcutaneously implanted with *LPCAT1*-gained A498 renal cancer cells. n = 8 for each group. Dox diet was given to mice after tumors were established at day 4 after implantation. Error bars represent SEM.

Statistical analysis was performed with two-way ANOVA plus a Tukey's multiple comparisons test for (C), (F) and (I), and one-way ANOVA with a Tukey's multiple comparisons test for (H). ***$p < 0.001$, **$p < 0.01$, *$p < 0.05$, NS, not significant.

See also Figure S6.

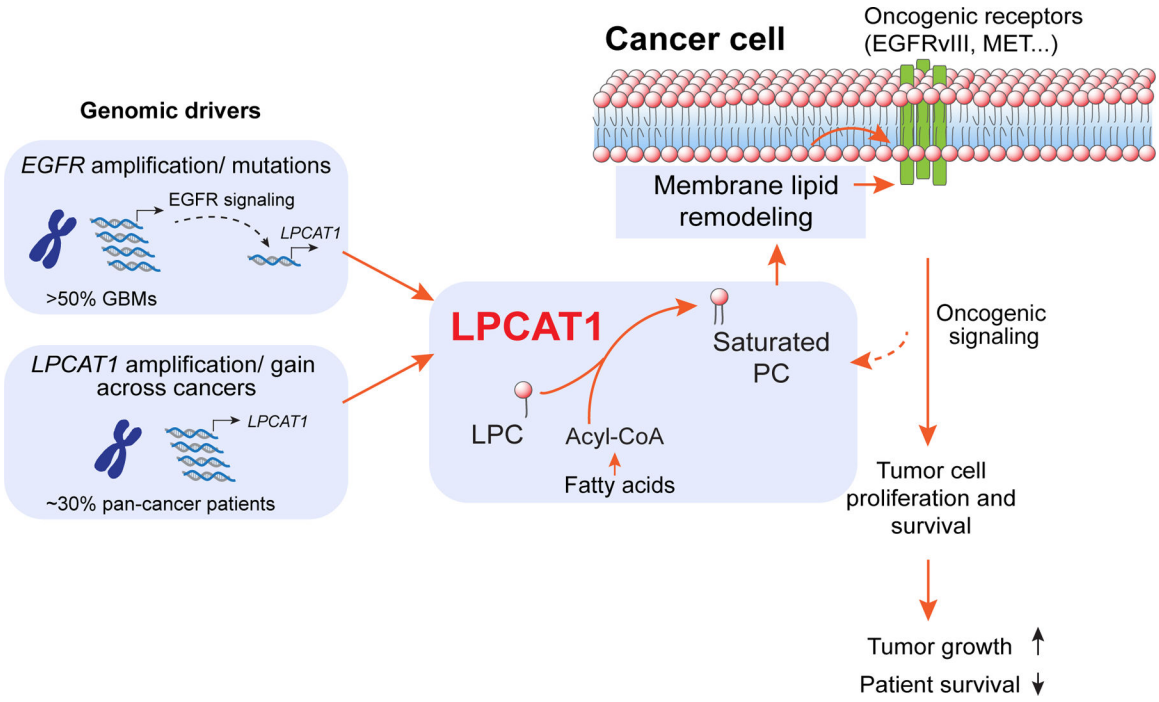

Figure 7. Proposed Model - LPCAT1 Links Genetic Alterations of Key Components of the Growth Factor Receptor Machinery with Plasma Membrane Remodeling to Drive Tumor Growth, Generating an Actionable Dependency across Cancers.

EGFR amplification/ mutations, the most common growth factor receptor alternations in cancer (over 50% in GBMs), upregulates *LPCAT1* and activates membrane lipid remodeling pathway in GBM. *LPCAT1* itself was also found frequently amplified across cancers, including lung cancers, ovarian cancers, bladder cancers, and invasive breast cancers, with a DNA copy-number increase in about 30% TCGA reported pan-cancer patients. Significant co-occurrence of genomic alternations between *LPCAT1* and genes in growth factor pathways was identified in TCGA pan-cancer datasets containing a total of 10,967 patient samples from 33 cancer types. LPCAT1-mediated phospholipid remodeling further supports the sustained oncogenic activity of grow factor receptors on plasma membrane of tumor cells both *in vitro* and *in vivo*, generating an actionable dependency across cancers.

KEY RESOURCES TABLE

REAGENT or RESOURCE	SOURCE	IDENTIFIER
Antibodies		
Rabbit Monoclonal anti-pEGFR-Y1068, Clone D7A5 (WB 1:1000, IHC 1:800)	Cell Signaling	Cat#3777; RRID:AB_2096270
Rabbit Polyclonal anti-LPCAT1 (WB 1:10000, IHC 1:100)	Proteintech	Cat#16112–1-AP; RRID:AB_2135554
Mouse Monoclonal anti-LPCAT1, Clone 8B6E9 (WB 1:10000)	Proteintech	Cat#66044–1-lg; RRID:AB_11045658
Rabbit Polyclonal anti-EGFR (WB 1:10000)	Millipore	Cat# 06–847; RRID:AB_2096607
mAb806 EGFRvIII antibody (IF 1:100)	Laboratory of Frank Furnari, UCSD	N/A
Mouse Monoclonal anti-EGFR (Ab-1), Clone 528 (Flow 1: 20)	Millipore	Cal#GR01; RRID:AB_564572
Rabbit Monoclonal anti-pAkt-S473, Clone D9E (WB 1:3000, IHC 1:50)	Cell Signaling	Cat#4060; RRID:AB_2315049
Rabbit Monoclonal anti-pNDRG1-T346, Clone D98G11 (WB 1:3000, IHC 1:100)	Cell Signaling	Cat#5482; RRID:AB_10693451
Rabbit Monoclonal anti-pS6-S235/236, Clone D57.2.2E (WB 1:3000, IHC 1:400)	Cell Signaling	Cat#4858; RRID:AB_916156
Rabbit Monoclonal anti-pMet-Y1234/1235, Clone D26 (WB 1:1000)	Cell Signaling	Cat#3077; RRID:AB_ 2143884
Rabbit Monoclonal anti-pERK-T202/Y204, Clone D13.14.4E (WB 1:2000)	Cell Signaling	Cat#4370; RRID:AB_2315112
Rabbit Monoclonal anti-pERK-T202/Y204, Clone 20G11 (IHC 1:100)	Cell Signaling	Cat#4376; RRID:AB_331772
Rabbit Monoclonal anti-Flotillin-1, Clone D2V7J (WB 1:1000)	Cell Signaling	Cat#18634; RRID:AB_2773040
Rabbit Monoclonal anti- Gα(q), Clone D5V1B (WB 1:1000)	Cell Signaling	Cat#14373; RRID:AB_2665457
Rabbit Monoclonal anti-p38 MAPK, Clone D13E1 (WB 1:1000)	Cell Signaling	Cal#8690; RRID:AB_10999090
Rabbit Monoclonal anti-Phospho-p38 MAPK (Thr180/Tyr182), Clone D3F9 (WB 1:1000)	Cell Signaling	Cat#4511; RRID:AB_2139682
Mouse Monoclonal anti-actin, Clone AC40 (WB 1:3000)	Sigma	Cat#A4700; RRID:AB_476730
Anti-rabbit IgG, HRP-linked (WB 1:3000)	Cell Signaling	Cat#7074; RRID:AB_2099233
Anti-mouse IgG, HRP-linked (WB 1:3000)	Cell Signaling	Cat#7076; RRID:AB_330924
Alexa Fluor anti-mouse 546 (IF 1:1000, Flow 1:500)	ThermoFisher Scientific	Cat#A11018; RRID:AB_2534085
Alexa Fluor anti-mouse 488 (IF 1:1000, Flow 1:500)	ThermoFisher Scientific	Cat#A11017; RRID:AB_2534084
Mouse Monoclonal anti-Ki67, Clone 8D5 (IHC 1:500)	Cell Signaling	Cat#9449 RRID:AB_2797703
Biological Samples		
GBM tumor tissue array	Guo et al., 2009	N/A
Chemicals, Peptides, and Recombinant Proteins		
DMEM	Corning	Cat#10–013
RPMI Medium 1640	Gibco	Cat#22400–089
DMEM/F12	Gibco	Cat#11320–033
Pen Strep Glutamine	Gibco	Cat#10378–016
Glutamax	Gibco	Cat#35050–061
B27	Gibco	Cat#17504–001

REAGENT or RESOURCE	SOURCE	IDENTIFIER
Fetal Bovine Serum (FBS)	Omega Scientific	Cat#FB-21
Tet-free Fetal Bovine Serum	Omega Scientific	Cat#FB-15
Epidermal Growth Factor (EGF)	Sigma	Cat#E9644
Fibroblast Growth Factor (FGF)	Sigma	Cat#F0291
Heparin	Sigma	Cat#H3149
AGM BulletKit	LONZA	Cat#CC-3186
PC16:0/16:0, 1,2-dipalmitoyl-sn-glycero-3-phosphocholine, DPPC	Avanti Polar Lipids	Cat#850355
PC16:0/18:1, 1-palmitoyl-2-oleoyl-sn-glycero-3-phosphocholine, POPC	Avanti Polar Lipids	Cat#850457
PC16:0/20:4, 1-palmitoyl-2-arachidonoyl-sn-glycero-3-phosphocholine, PAPC	Avanti Polar Lipids	Cat#850459
16:0 Lyso PC	Avanti Polar Lipids	Cat#855675
Fatty acid free Bovine Serum Albumin	Sigma	Cat#A6003
Sodium palmitate	Sigma	Cat#P9767
Sodium myristate	Sigma	Cat#M8005
Sodium stearate	Sigma	Cat#S3381
Arachidonic acid sodium salt	Sigma	Cat#A8798
Sodium oleate	Sigma	Cat#O7501
Sodium stearate	Sigma	Cat#S3381
Linoleic acid sodium salt	Sigma	Cat#L8134
Erlotinib	Selleckchem	Cat#S1023
Low gelling temperature agarose	Sigma	Cat#A9045
Trypan Blue Solution	Gibco	Cat#15250061
Doxycycline	Sigma	Cat#D9891
Dox diet	Bio-Serv	Cat#S3888
Matrigel Basement Membrane Matrix	Corning	Cat#356234
Opti-Prep Density Gradient Medium	Sigma	Cat#D1556
rTdT	Invitrogen	Cat#10533065
Digoxigenin-11-dUTP	Roche	Cat#11558706910
Anti-Digoxigenin-POD	Roche	Cat#11207733910
Crystal violet solution	Sigma	Cat#V5265
Laurdan (6-Dodecanoyl-2-Dimethylaminonaphthalene)	ThermoFisher Scientific	Cat#D250
Critical Commercial Assays		
Lipofectamine RNAiMAX Transfection Reagent	ThermoFisher Scientific	Cat#13778150
X-tremeGENE HP DNA Transfection Reagent	Roche	Cat#6366236001
RNeasy Mini Kit	QIAGEN	Cat#74106
SYBR Green Supermix	Bio-Rad	Cat#1708880
BCA Protein Assay Kit	ThermoFisher Scientific	Cat#23225
SuperSignal West Pico PLUS Chemiluminescent Substrate	ThermoFisher Scientific	Cat#34580
FITC Annexin V Apoptosis Detection Kit I	BD Biosciences	Cat#556547

REAGENT or RESOURCE	SOURCE	IDENTIFIER
Experimental Models: Cell Lines		
Human: U87	ATCC	HTB-14
Human: U87EGFRvIII	Wang et al., 2006	N/A
Human: GBM39 patient-derived neurosphere cells	Nathanson et al., 2014	N/A
Human: HK301 patient-derived neurosphere cells	Laboratory of Harley Kornblum, UCLA	N/A
Human: H1437	ATCC	CRL-5872
Human: H1734	ATCC	CRL-5891
Human: HCC1954	ATCC	CRL-2338
Human: H1650	ATCC	CRL-5883
Human: T47D	ATCC	HTB-133
Human: PC-9	ATCC	RRID:CVCL_B260
Human: A549	ATCC	CCL-185
Human: Capan1	ATCC	HTB-79
Human: CAOV3	ATCC	HTB-75
Human: OVCAR3	ATCC	HTB-161
Human: OVCAR8	ATCC	RRID:CVCL_1629
Human: SKMEL5	ATCC	HTB-70
Human: YAPC	DSMZ	RRID:CVCL_1794
Human: A498	ATCC	CRL-7908
Human: Caki1	ATCC	HTB-46
Human: DU145	ATCC	HTB-81
Human: PC-3	ATCC	CRL-1435
Human: SN12C	ATCC	RRID:CVCL_1705
Human: H23	ATCC	CRL-5800
Human: IMR90	ATCC	CCL-186
Human: RPE1	ATCC	CRL-4000
Human: Normal Human Astrocyte (NHA)	LONZA	CC-2565
Experimental Models: Organisms/Strains		
Mouse: Athymic Nude Foxn1nu	Charles River Laboratories	Strain 490
Oligonucleotides		
SMARTpool: ON-TARGETplus human LPCAT1 siRNA	Dharmacon	Cat#L-010289–00-0010
Non-targeting negative control siRNA	Life technologies	Cat#4390844
LPCAT1 FISH probe	Empire Genomics	Cat. LPCAT1–20-RE
Recombinant DNA		
pLVX-Puro Vector	Clontech	Cat#632159
pLVX-Puro-Flag-LPCAT1	This study	N/A
pLVX-Puro-rLPCAT1 (shRNA resistant)	This study	N/A
pLVX-puro-HA-AKT-E17K-CA	This study	N/A
SMARTvector Inducible Human LPCAT1 shRNA #1	Dharmacon	Cat#V3SH11252–224825213

REAGENT or RESOURCE	SOURCE	IDENTIFIER
SMARTvector Inducible Human LPCAT1 shRNA #2	Dharmacon	Cat#V3SH11252–230837417
SMARTvector Inducible non-targeting shRNA	Dharmacon	Cat#VSC11657
LPCAT1 #1 shRNA	Sigma	TRCN0000056068
LPCAT1 #2 shRNA	Sigma	TRCN0000231881
LPCAT1 #3 shRNA	Sigma	TRCN0000231878
Non-targeting control shRNA Targeting sequence: 5'-CTTACGCTGAGTACTTCGA-3'	This study	N/A
LPCAT1 qPCR forward primer: 5'TTGCCGCTGCCATGATGCTG3'	This study	N/A
LPCAT1 qPCR reverse primer: 5'AACCTTCCTCCACAGGGCCG3'	This study	N/A
Software and Algorithms		
Image Lab Software	Bio-Rad	RRID:SCR_014210
GraphPad Prism7	GraphPad Software	RRID:SCR_000306
Cytoscape	Shannon et al., 2003	RRID:SCR_003032
ImageJ	NIH	RRID:SCR_003070
Kaluza Analysis Software	Beckman Coulter	RRID:SCR_016182
Leica LAS software	Leica	RRID:SCR_013673
Visiopharm	Visiopharm	https://www.visiopharm.com/
cBioProtal	Cerami et al., 2012; Gao et al., 2013	http://www.cbioportal.org/
GEPIA	Tang et al., 2017	http://gepia.cancer-pku.cn/
Agilent MassHunter Quantitative Analysis Software (version B.05.00)	Agilent	RRID:SCR_015040